UNIVERSITY OF CALIFORNIA, SAN DIEGO

Pathways and Cell Types Underlying Visual Perception in the Mouse

A dissertation submitted in partial satisfaction of the requirements for the degree Doctor of Philosophy

in

Neurosciences

by

Ashley Lauren Juavinett

Committee in charge:

Professor Edward Callaway, Chair
Professor Andrew Huberman, Co-Chair
Professor Takaki Komiyama
Professor Jaime Pineda
Professor John Reynolds
Professor John Serences

2016

The Dissertation of Ashley Lauren Juavinett is approved, and is acceptable in quality and form for publication on microfilm and electronically:

Co-Chair

Chair

University of California, San Diego

2016

DEDICATION

To my parents, who have supported my curiosity and education since the very beginning.

To Beth, an endless source of mentorship, inspiration, and culinary experiences.

To the teachers along the way, who shaped my early ideas about how the brain (and world) works.

To Catherine, whose unconditional love and natural brilliance perpetually guides and motivates me.

To my friends in San Diego and elsewhere,
for camaraderie and connection across years and distance.

EPIGRAPH

For the time being, we can only babble some interpretative, timid, conjectural explanations, almost always premature, which certain discontented readers, very influenced by rigorous demonstrations, will find entirely fruitless. Certainly, we shall not negate how weak and ill-founded are many of our speculations, and how much they are in need of modification, rectification or even substitution. But hypotheses in Science, even erroneous ones, have an important goal. This aim is not always to formulate a truth, but to indicate the path to an investigation. They are, above all, *great awakeners of souls*, because they agitate the moral environment (that dead sea of the routine which is fatal to all progress), stimulate the spirit of doubt and contradiction, so much developed in laboratory men, and are the starting point of new and fruitful observations and experiments.

– SANTIAGO RAMÓN Y CAJAL
Textura del Sistema Nervioso del Hombre y de los Vertebrados

TABLE OF CONTENTS

LIST OF FIGURES AND TABLES

ACKNOWLEGEMENTS

First and foremost, I would like to acknowledge Ed Callaway as my advisor and co-chair of my thesis committee. His guidance and insight throughout each of these projects has been truly invaluable.

In addition, I would like to thank my thesis committee, comprised of Andrew Huberman, John Reynolds, Takaki Komiyama, John Serences, and Jaime Pineda. Their advice has shaped each of these projects as well as my graduate school experience.

I would also like to acknowledge the collective knowledge and support from the Callaway Lab and UCSD Neurosciences Program. I have benefitted tremendously from such an active community of clever minds.

Chapter 1, in full, is a reprint of the material as it appears in Juavinett, A.L. & Callaway, E.M. (2015) *Current Biology* 25(13): 1759-64. The dissertation author was the primary author of this paper.

Chapter 2, in part, is a reprint of the material as it appears in Kim. E.J., Juavinett, A.L., Kyubwa, E.M., Jacobs, M.W., Callaway, E.M. (2015). Three Types of Cortical Layer 5 Neurons That Differ in Brain-wide Connectivity and Function. *Neuron* 88(6): 1253-67. The dissertation author was the second author in this collaborative effort.

VITA

2011 B.S., Neuroscience, Lafayette College, Easton, PA

2012 Teaching Assistant, Neurosciences Program, UC San Diego

2015 Instructor, Department of Psychology, UC San Diego

2016 Ph.D., Neurosciences, UC San Diego

PUBLICATIONS

Juavinett, A.L., Nauhaus, I., Garrett, M., Callaway, E.M. Automated identification of mouse visual areas with intrinsic signal imaging. *Submitted to Nature Protocols.*

Kim. E.J., **Juavinett, A.L**., Kyubwa, E.M., Jacobs, M.W., Callaway, E.M. (2015). Three Types of Cortical Layer 5 Neurons That Differ in Brain-wide Connectivity and Function. *Neuron* 88(6): 1253-67.

Juavinett, A.L., Callaway, E.M. (2015). Pattern and Component Motion Responses in Mouse Visual Cortex. *Current Biology* 25(13): 1759-64.

Stewart, J.L., **Juavinett, A.L**., May, A.C., Davenport, P.W., Paulus, M.P. (2015). Do You Feel Alright? Attenuated Neural Processing of Aversive Interoceptive Stimuli in Current Stimulant Users. *Psychophysiology* 52(2): 249-62.

Pineda, J.A., **Juavinett, A.L**., Datko, M. (2012). Self-regulation of brain oscillations as a treatment for aberrant brain connections in children with autism. *Medical Hypotheses 79*(6): 790-8.

AWARDS

2016 UCSD Neuroscience Excellence in Graduate Teaching Award

2013 National Science Foundation Graduate Research Fellowship

2012 National Science Foundation GK-12 Grant

ABSTRACT OF THE DISSERTATION

Pathways and Cell Types Underlying Visual Perception in the Mouse

by

Ashley Lauren Juavinett

Doctor of Philosophy in Neuroscience

University of California, San Diego, 2016

Professor Edward M. Callaway, Chair

Professor Andrew Huberman, Co-Chair

The primary challenge of systems neuroscience is identifying the circuits and cell types that underlie sensation and behavior. Faced with the daunting task of unraveling six layers of cortex, a hierarchy of visual areas, and a multitude of cell types, visual neuroscience relies on innovative technologies to achieve a circuit-level understanding of perceptual phenomena. This dissertation aims to be an extension of this effort by using advanced tools to address several longstanding questions regarding the structure and function of the visual system.

In the past decade, mouse visual cortex has come to the forefront of systems neuroscience, serving as a common ground to study the role of cell types in behavior. Armed with a remarkable arsenal of genetic and molecular tools in transgenic mice, we are poised to observe and manipulate visual circuits in a cell-type specific manner. Yet doing so requires a comprehensive understanding of the system at hand. In the work presented here, I extend our knowledge of the mouse visual system so that we may exploit its experimental advantages to address circuit-level questions.

Spanning multiple techniques and circuits, this dissertation investigates the mouse visual system from several angles. First, it refines our understanding of mouse visual cortex functional organization with bulk loaded calcium indicators and a well-studied higher-order stimulus, moving plaids (Chapter 1). Secondly, it characterizes the functional response properties of three different genetically defined layer 5 cell types, using *in vivo* two-photon imaging in the primary visual cortex (Chapter 2). Lastly, it delineates the topography of thalamocortical projections from the secondary visual thalamic nucleus (LP) to multiple visual cortical areas with classic tracing methods as well as novel viral combinations (Chapter 3). Together, these three studies advance our understanding of the connectivity and function of the mouse visual system, bringing us closer to bridging neurons and behavior.

INTRODUCTION

Over 100 years ago, Santiago Ramón y Cajal took his first historic looks onto Golgi stained tissue, concluding that the neuron was the primary unit of computation in the nervous system. Yet Ramón y Cajal himself recognized that his observations were limited, even describing them as “simple” and “infantile.” He yearned for functional, mechanistic explanations, calling on future neuroscientists to seek more dynamic explanations for animal behavior (Ramón y Cajal, 1904).

Since the time of Ramón y Cajal, neuroscientists have been pouring over images and recordings of neurons, hoping to connect this fundamental unit to behaviors that are fundamentally human. As in all scientific endeavors, technology shapes the extent to which we can make these connections. The past century has seen an incredible surge of anatomical and functional techniques to study the brain, beginning with early histology, electron microscopy, and single-cell electrophysiology, and advancing with viral tracing, electrode array recording, calcium imaging, and optogenetics (Boyden et al., 2005; Buzsáki, 2004; Callaway, 2005; Chen et al., 2013; Du et al., 2011; Luo et al., 2008; Sejnowski et al., 2014). We are at an unprecedented time in neuroscience, when the tools to simultaneously observe and manipulate specific populations of neurons – predominantly in mice – are producing a barrage of insights into age-old questions about connectivity and function (Buzsáki et al., 2015; Okun et al., 2016; Packer et al., 2014; Vandecasteele et al., 2012). Already, various groups have capitalized on the methodological advantages afforded by the mouse model to address circuit-level questions of visual perception and beyond (e.g.

Adesnik et al., 2013; Cruz-Martín et al., 2015; Komiyama et al., 2010; Peters et al., 2014; Lee et al., 2012; Lien and Scanziani, 2013; Nienborg et al., 2013).

In this spirit of connecting structure to function using innovative techniques, my dissertation applies our understanding of primate and carnivore brains to the mouse, with the ultimate goal of extrapolating circuit-level insights back to humans. Empowered by a longstanding tradition of exploiting the visual system for its experimental tractability, I focus here on the connectivity and function of the visual cortex and related nuclei in the thalamus.

Circuits for visual perception

An abundant history of visual neuroscience, including Barlow (1953), Hubel and Wiesel (1962; 1959), and Felleman and Van Essen (1991), has endowed us with a rigorous understanding of visual pathways in carnivores and primates. Visual information first encounters a mosaic of photoreceptors and ganglion cells in the retina, and is then passed through the optic chiasm to the lateral geniculate nucleus (LGN) of the thalamus. In anatomically and functionally separate channels, visual information then arrives in layer 4 of primary visual cortex (V1). After reaching V1, information is passed to a variety of different extrastriate regions, as well as back to the secondary visual nucleus, known as the pulvinar or lateral posterior nucleus (LP) in mice. In addition, there is a tremendous amount of feedback from cortex to LGN. Alternatively, information from the retina can be passed on to the superior colliculus (SC), to LP/pulvinar, and then to various parts of cortex, a route known as the extrageniculate pathway.

Visual processing after V1 is traditionally divided into parallel dorsal and ventral streams, primarily involved in action-oriented, motion computations ("where), or object-recognition ("what"), respectively (Felleman and Van Essen, 1991; Goodale and Milner, 1992; Ungerleider, 1994; Ungerleider and Mishkin, 1982). Several of these extrastriate areas have incredibly specific functions, such as motion perception in the middle temporal area (MT; Allman and Kaas, 1971; Born and Bradley, 2005; Dubner and Zeki, 1971), and face perception in the fusiform face area (FFA; Kanwisher et al., 1997; Tsao et al., 2006).

Mapping the organization and function of these visual areas onto rodents has been the primary challenge in utilizing the mouse model of vision. In Chapter 1, I extend our characterization of these dorsal and ventral streams to the mouse system, building on the recent body of work investigating the functional specialization of mouse visual areas (e.g. Andermann et al., 2011; Glickfeld et al., 2014; Huberman and Niell, 2011; Marshel et al., 2011; Niell and Stryker, 2008; Niell, 2011).

Mouse visual cortex

The fundamental organization of the mouse visual system is quite similar to that of primates and carnivores (Huberman and Niell, 2011). As in the primate, visual information relayed through the LGN first reaches cortex in V1, where it is then sent to multiple interconnected extrastriate regions (Glickfeld et al., 2013; Polack and Contreras, 2012). While mice are afoveal and have lower resolution vision than primates (Prusky et al., 2000), they still heavily use vision to navigate the world (Chen et al., 2013). Indeed, behavioral studies have shown that they can discriminate the direction of randomly moving dots (Douglas et al., 2006), recognize 3D objects from

2D images (Zoccolan et al., 2009) and detect changes in orientation (Glickfeld et al., 2013; Lee et al., 2012). Recently, several groups have shown that mice can perform cross-modal and visual attention tasks (Kim et al., 2016; Wimmer et al., 2015).

Similar to primate cortex, mouse visual cortex is organized retinotopically (Wagor et al., 1980), selective for orientation and direction (Niell and Stryker, 2008; Sohya et al., 2007), structured with ON/OFF receptive fields (Smith and Häusser, 2010), and surrounded by multiple extrastriate areas that are likely involved in higher-order visual processing (Andermann et al., 2011; Garrett et al., 2014; Marshel et al., 2011; Wang and Burkhalter, 2007). Mice have at least eleven retinotopically-defined visual areas (Andermann et al., 2011; Garrett et al., 2014; Marshel et al., 2011; Wang and Burkhalter, 2007). These areas are retinotopically organized but small, and are best identified using intrinsic signal optical imaging (Garrett et al., 2014).

Anatomical and functional evidence suggests that there are parallel routes of information through mouse visual cortex, akin to the dorsal and ventral streams in primates (Gao et al., 2010; Glickfeld et al., 2013a; Wang et al., 2011; 2012). The lateromedial area (LM), just lateral to V1, is homologous to primate V2, receiving V1 input and passing it on to other extrastriate regions such as AM or RL (Kalatsky and Stryker, 2003; Rosa and Krubitzer, 1999). A subset of areas, LM, AL, RL, and AM, have high direction selectivity coupled with preferences for high temporal frequency and low spatial resolution, making them candidates for a functional dorsal, movement-sensitive stream of information (Marshel et al., 2011; Andermann et al., 2011). In addition, RL has been identified as a somatosensory integration region (Olcese et al., 2013), and PM may be involved in scene recognition and navigation (Roth et al., 2012).

It is unknown whether these areas generate higher-order functional specializations like those in the primate visual system. I wished to challenge this system with more complicated stimuli to further assess its potential for elucidating circuit mechanisms of complex behaviors. I therefore turned to the plaid stimulus, which has proved useful for untangling the circuits involved in visual motion perception in cats and monkeys for the past 30 years (Movshon et al., 1985).

Cells for complex motion perception

Over the years, several different stimuli have been used to probe motion perception, most notably drifting plaids and stochastic moving dots (Movshon et al., 1985; Newsome and Paré, 1988; Stoner and Albright, 1992). Plaids are composed of two overlaid drifting gratings, typically offset by 60 to 90 degrees (Adelson and Movshon, 1982). When these gratings are presented at similar contrast, spatial frequency, and temporal frequency, and with intersections of a realistic luminance, they cohere into a percept of one moving plaid (Adelson and Movshon, 1982; Delicato and Derrington, 2005; Stoner et al., 1990). Cells respond to plaid stimuli on a continuum from “component” cells, responding only to the individual gratings, to “pattern” cells, responding only to the global motion of the plaid (Movshon et al., 1985). Lesion studies in macaques suggest that these cells underlie the animal’s ability to integrate local motions into a coherent moving object (Newsome and Paré, 1988; Rudolph and Pasternak, 1999).

It is likely that plaid motion perception occurs in two steps, with component cells in V1 first recognizing local motion, and cells in MT nonlinearly filtering and integrating these inputs to a compute a global motion (Rust et al., 2006; Simoncelli &

Heeger, 1998). In support of this hypothesis, the quantity of pattern cells increases as visual information moves up the hierarchy. While there are sparse pattern cell responses in primate V1 (Tinsley et al., 2003; Khawaja et al., 2009), 25-30% of cells in MT and 40-60% in MST are pattern direction selective (Movshon et al., 1985; Khawaja et al., 2013).

Evidence for pattern motion selectivity has been observed in blowflies (Saleem et al., 2012), cats (Movshon et al., 1985), primates (Khawaja et al., 2013, 2009; Tinsley et al., 2003), and humans (Huk and Heeger, 2002). To date, the observation of pattern cell responses in mouse cortex has not been reported. Therefore, in order to probe the mouse visual system for complex motion processing and enable circuit-level investigations into the mechanisms that may enable such computations, I characterized the visual responses to plaids in five different mouse visual cortical regions (Chapter 1). To do so, I employ intrinsic signal imaging to generate retinotopic maps and target a bulk-loaded calcium indicator. As fully described in Chapter 1, several regions of mouse extrastriate cortex have cells that can compute pattern motion, further delineating dorsal and ventral streams in mice.

How areas such as MT develop such specific roles in visual processing – whether they are computed *de novo* within an area, or rather computed sequentially from area to area – is an open question that could be significantly aided by the ability to study cells with known projections. For instance, if we could specifically target cells that project to a dorsal stream area and investigate the information represented by these cells, we could better understand information transfer through the visual pathway. Antidromic stimulation has provided some insight into this question; for example, V1 cells that project to MT are direction selective (Movshon and Newsome,

1996). Still, there are additional open questions about the roles of cortical cells that project to other cortical areas versus subcortical areas such as SC. In Chapter 2, I address this question by targeting cells with known projections to cortical or subcortical areas, finding that they do indeed encode different visual information.

Cortical layers: connectivity and function

One of Ramón y Cajal's first observations about the cortex was its diversity of cell shapes and its apparent laminar structure (Ramón y Cajal, 1904). Within cortex, excitatory and inhibitory cells can be classified by their morphology, intrinsic physiology, synaptic targets, or the presence of calcium-binding proteins, many of which have been capitalized on for the generation of Cre driver lines (Taniguchi et al., 2011). Composing approximately 30% of the rodent cortex, GABAergic neurons are a prevalent and extremely diverse group of cells (Bloom and Iversen, 1971) with important roles in visual perception (e.g. Adesnik et al., 2013; Nienborg et al., 2013) and differential patterns of input from superficial or deep layers of cortex (Wall et al., 2016).

In addition, it is useful to characterize cells based on their laminar location, as this is often indicative of the neuron's role in information integration or distribution. Information from the thalamus is sent to layer 4 of cortex, which passes this information onto layers 2 and 3, and eventually onto 5 and 6 (Callaway, 1998; Harris and Mrsic-Flogel, 2014). Layer 5 provides the primary output to subcortical structures such as the striatum and superior colliculus (Bourassa and Deschênes, 1995; Callaway, 1998). Similar to the array of Cre-recombinase transgenic mouse lines that have enabled studies of inhibitory cells, there are an increasing number of lines that

mark cells in a specific layer of cortex (Harris et al., 2014; Taniguchi et al., 2011). However, there are very few known Cre driver lines that specifically mark a population of cells with known projection patterns (Gong et al., 2007).

Recently, our lab has described three different layer 5 cell types that can be targeted with transgenic mice that are available in the GENSET database. In line with known properties of these layer 5 cells in primates, they differ in morphology, connectivity, and intrinsic firing properties (Kim et al., 2015). However, without an effective way to selectively study these cells, their function has remained elusive. In Chapter 2, I selectively express the genetically-encoded calcium indicator GCaMP6 in these cells to functionally characterize them, investigating whether a cell's target structure can be correlated with its visual response properties. I demonstrate that these three cell types have unique visual receptive fields, bridging structure and function in mouse visual cortex. This work also opens up a means of testing the contributions of these cell types to other cortical and subcortical areas.

Thalamocortical loops through LP/pulvinar

A major target of subcortically projecting visual cortex neurons is the secondary visual nucleus, LP/pulvinar. Pulvinar is a brain region with multiple ascribed roles, most notably attention (e.g. Desimone et al., 1990; Jahn et al., 2012; Snow et al., 2009; Zhou et al., 2016). Although much speculation centers on the role of the pulvinar's reciprocal connectivity with cortex (Crick and Koch, 1998; Olshausen et al., 1993; Shipp, 2003), a precise connectivity map of inputs and outputs does not exist, and would greatly inform conjectures about its function. Specifically, do these

loops route information through the visual hierarchy, or are they simply redundant loops to cortex that serve some other purpose, such as synchronization?

In the mouse, LP has just begun to regain attention (Allen et al., 2016; Lawrence and Studholme, 2014; Roth et al., 2015; Tohmi et al., 2014). Still, despite a body of research describing the organization of LP in rats, hamsters, squirrels, and cats (Baldwin et al., 2011; Crain and Hall, 1980; Hughes, 1977; Kamishina et al., 2008; Mason, 1978; Takahashi, 1985), the topographical organization of thalamocortical projections in mouse LP has not been fully described. Constructing an input-output connectivity map of mouse LP depends on an understanding of its topography. Therefore, the first step to investigating the role of mouse LP is a concrete understanding of the organization of its inputs to cortex.

To address this question, I employ various combinations of tracing methods to investigate the precise connectivity between the visual thalamus and cortex (Chapter 3). The bulk of this investigation uses cholera toxin subunit B, a protein retrograde tracer, to investigate the organization of thalamocortical projections. In addition, I inject a combination of a retrograde and anterograde virus to identify the axonal patterns of cells in thalamus with a known projection target. Both of these approaches demonstrate a clear topographical organization and remarkable specificity in the projections from LP to cortex, and invite further questions about the input to these cells.

Where truth meets usefulness

Ultimately, the hope of this dissertation research and of many in the field is that the insights gained here might lead to a deeper understanding of the human

condition, both typical and atypical. Human cortex is organized very similarly to mouse and primate cortex, with many of the same inhibitory cell markers. In fact, many of these markers have been implicated in neurological disorders (e.g. CCK; Blum and Mann, 2002; Bourin et al., 1996; Wang et al., 1984; Zhang et al., 2000). At a systems level, abnormal functioning in cortical circuits likely underlies many sensory disorders, including autism and schizophrenia (Courchesne et al., 2007; Spencer et al., 2003; Vissers et al., 2012). With a deeper understanding of how structure and function interact in a small mammalian brain, we may ultimately be able to pinpoint how such circuits go awry in humans. In Ramòn y Cajal's words, "We long indeed for a happier time for the individual and the entire human kind when truth and usefulness will become one and the same thing" (Cajal, 1904).

References

Adelson, E.H., Movshon, J.A., 1982. Phenomenal coherence of moving visual patterns. Nature 300, 523–525.

Adesnik, H., Bruns, W., Taniguchi, H., Huang, Z.J., Scanziani, M., 2013. A neural circuit for spatial summation in visual cortex. Nature 490, 226–231.

Allen, A.E., Procyk, C.A., Howarth, M., Walmsley, L., Brown, T.M., 2016. Visual input to the mouse lateral posterior and posterior thalamic nuclei: photoreceptive origins and retinotopic order. J. Physiol. 594, 1911–1929. doi:10.1113/JP271707

Allman, J.M., Kaas, J.H., 1971. A representation of the visual field in the caudal third of the middle temporal gyrus of the owl monkey (Aotus trivirgatus). Brain Res. 31, 85–105. doi:10.1016/0006-8993(71)90635-4

Andermann, M.L., Kerlin, A.M., Roumis, D.K., Glickfeld, L.L., Reid, R.C., 2011. Functional Specialization of Mouse Higher Visual Cortical Areas. Neuron 72, 1025–1039. doi:10.1016/j.neuron.2011.11.013

Baldwin, M.K.L., Wong, P., Reed, J.L., Kaas, J.H., 2011. Superior colliculus connections with visual thalamus in gray squirrels (Sciurus carolinensis): evidence for four subdivisions within the pulvinar complex. J. Comp. Neurol. 519, 1071–1094.

Barlow, H.B., 1953. Summation and inhibition in the frog's retina. J. Physiol. 119, 69–88. doi:10.1113/jphysiol.1953.sp004829

Bloom, F.E., Iversen, L.L., 1971. Localizing 3H-GABA in nerve terminals of rat cerebral cortex by electron microscopic autoradiography. Nature 229, 628–630. doi:10.1038/229628a0

Blum, B.P., Mann, J.J., 2002. The GABAergic system in schizophrenia. Int. J. Neuropsychopharmacol. 5, 159–179. doi:10.1017/S1461145702002894

Bourassa, J., Deschênes, M., 1995. Corticothalamic projections from the primary visual cortex in rats: a single fiber study using biocytin as an anterograde tracer. Neuroscience 66, 253–263. doi:10.1016/0306-4522(95)00009-8

Bourin, M., Malinge, M., Vasar, E., Bradwejn, J., 1996. Two faces of cholecystokinin: anxiety and schizophrenia. Fundam. Clin. Pharmacol. 10, 116–26.

Boyden, E.S., Zhang, F., Bamberg, E., Nagel, G., Deisseroth, K., 2005. Millisecond-timescale, genetically targeted optical control of neural activity. Nat. Neurosci. 8, 1263–1268. doi:10.1038/nn1525

Buzsáki, G., 2004. Large-scale recording of neuronal ensembles. Nat. Neurosci. 7, 446–451. doi:10.1038/nn1233

Buzsáki, G., Stark, E., Berényi, A., Khodagholy, D., Kipke, D.R., Yoon, E., Wise, K.D., 2015. Tools for probing local circuits: High-density silicon probes combined with optogenetics. Neuron. doi:10.1016/j.neuron.2015.01.028

Cajal, S.R., 1904. Textura del Sistema Nervioso del Hombre y de los Vertebrados. Springer Vienna, Moya, Madrid.

Callaway, E.M., 2005. A molecular and genetic arsenal for systems neuroscience. Trends Neurosci. 28, 196–201.

Callaway, E.M., 1998. LOCAL CIRCUITS IN PRIMARY VISUAL CORTEX OF THE MACAQUE MONKEY. Annu. Rev. Neurosci 21, 47–74.

Chen, G., King, J.A., Burgess, N., O'Keefe, J., 2013. How vision and movement combine in the hippocampal place code. Proc. Natl. Acad. Sci. 110, 378–383.

Chen, T.-W., Wardill, T.J., Sun, Y., Pulver, S.R., Renninger, S.L., Baohan, A., Schreiter, E.R., Kerr, R.A., Orger, M.B., Jayaraman, V., Looger, L.L., Svoboda, K., Kim, D.S., 2013. Ultrasensitive fluorescent proteins for imaging neuronal activity. Nature 499, 295–300.

Courchesne, E., Pierce, K., Schumann, C.M., Redcay, E., Buckwalter, J.A., Kennedy, D.P., Morgan, J., 2007. Mapping early brain development in autism. Neuron 56, 399–413. doi:10.1016/j.neuron.2007.10.016

Crain, B.J., Hall, W.C., 1980. The normal organization of the lateral posterior nucleus of the golden hamster. J. Comp. Neurol. 193, 351–370.

Crick, F., Koch, C., 1998. Constraints on cortical and thalamic projections: the no-strong-loops hypothesis. Nature 391, 245–250.

Cruz-Martín, A., El-Danaf, R.N., Osakada, F., Sriram, B., Dhande, O.S., Nguyen, P.L., Callaway, E.M., Ghosh, A., Huberman, A.D., 2015. A dedicated circuit links direction-selective retinal ganglion cells to the primary visual cortex. Nature 507, 358–361.

Delicato, L.S., Derrington, A.M., 2005. Coherent motion perception fails at low contrast. Vision Res. 45, 2310–2320.

Desimone, R., Wessinger, M., Thomas, L., Schneider, W., 1990. Attentional Control of Visual Perception: Cortical and Subcortical Mechanisms. Cold Spring Harb. Symp. Quant. Biol. 55, 963–971.

Douglas, R.M., Neve, A., Quittenbaum, J.P., Alam, N.M., Prusky, G.T., 2006. Perception of visual motion coherence by rats and mice. Vision Res. 46, 2842–2847.

Du, J., Blanche, T.J., Harrison, R.R., Lester, H.A., Masmanidis, S.C., 2011. Multiplexed, High Density Electrophysiology with Nanofabricated Neural Probes.

PLoS One 6, e26204. doi:10.1371/journal.pone.0026204

Felleman, D.J., Van Essen, D.C., 1991. Distributed hierarchical processing in the primate cerebral cortex. Cereb. Cortex 1, 1–47.

Garrett, M.E., Nauhaus, I., Marshel, J.H., Callaway, E.M., 2014. Topography and areal organization of mouse visual cortex. J. Neurosci. 34, 12587–12600.

Glickfeld, L.L., Andermann, M.L., Bonin, V., Reid, R.C., 2013. Cortico-cortical projections in mouse visual cortex are functionally target specific. Nat. Neurosci. 16, 219–226.

Glickfeld, L.L., Histed, M.H., Maunsell, J.H.R., 2013. Mouse Primary Visual Cortex Is Used to Detect Both Orientation and Contrast Changes. J. Neurosci. 33, 19416–19422. doi:10.1523/JNEUROSCI.3560-13.2013

Glickfeld, L.L., Reid, R.C., Andermann, M.L., 2014. A mouse model of higher visual cortical function. Curr. Opin. Neurobiol. 24, 28–33.

Gong, S., Doughty, M., Harbaugh, C.R., Cummins, A., Hatten, M.E., Heintz, N., Gerfen, C.R., 2007. Targeting Cre Recombinase to Specific Neuron Populations with Bacterial Artificial Chromosome Constructs. J. Neurosci. 27, 9817–9823. doi:10.1523/JNEUROSCI.2707-07.2007

Goodale, M.A., Milner, A.D., 1992. Separate visual pathways for perception and action. Trends Neurosci. 15, 20–25. doi:10.1016/0166-2236(92)90344-8

Harris, J.A., Hirokawa, K.E., Sorensen, S.A., Gu, H., Mills, M., Ng, L.L., Bohn, P., Mortrud, M., Ouellette, B., Kidney, J., Smith, K.A., Dang, C., Sunkin, S., Bernard, A., Oh, S.W., Madisen, L., Zeng, H., 2014. Anatomical characterization of Cre driver mice for neural circuit mapping and manipulation. Front. Neural Circuits 8.

Harris, K.D., Mrsic-Flogel, T.D., 2014. Cortical connectivity and sensory coding. Nature 503, 51–58.

Hubel, D.H., Wiesel, T.N., 1962. Receptive fields, binocular interaction and functional architecture in the cat's visual cortex. J. Physiol. 160, 106–154.

HUBEL, D.H., WIESEL, T.N., 1959. Receptive fields of single neurones in the cat's striate cortex. J. Physiol. 148, 574–91.

Huberman, A.D., Niell, C.M., 2011. What can mice tell us about how vision works? Trends Neurosci. 34, 464–473.

Hughes, H.C., 1977. Anatomical and neurobehavioral investigations concerning the thalamo-cortical organization of the rat's visual system. J. Comp. Neurol. 175, 311–36. doi:10.1002/cne.901750306

Huk, A.C., Heeger, D.J., 2002. Pattern-motion responses in human visual cortex. Nat.

Neurosci. 5, 72–75.

Jahn, H.M., Neumeyer, A., Saalmann, Y.B., Pinsk, M.A., Wang, L., Li, X., Kastner, S., 2012. The pulvinar regulates information transmission between cortical areas based on attention demands. Science (80-.). 337, 753–756.

Kalatsky, V.A., Stryker, M.P., 2003. New paradigm for optical imaging: temporally encoded maps of intrinsic signal. Neuron 38, 529–545.

Kamishina, H., Yurcisin, G.H., Corwin, J. V, Reep, R.L., 2008. Striatal projections from the rat lateral posterior thalamic nucleus. Brain Res. 1204, 24–39.

Kanwisher, N., McDermott, J., Chun, M.M., 1997. The fusiform face area: a module in human extrastriate cortex specialized for face perception. J. Neurosci. 17, 4302–11.

Khawaja, F.A., Liu, L.D., Pack, C.C., 2013. Responses of MST neurons to plaid stimuli. J. Neurophysiol. 110, 63–74.

Khawaja, F.A., Tsui, J.M.G., Pack, C.C., 2009. Pattern Motion Selectivity of Spiking Outputs and Local Field Potentials in Macaque Visual Cortex. J. Neurosci. 29, 13702–13709.

Kim, E.J., Juavinett, A.L., Kyubwa, E.M., Jacobs, M.W., Callaway, E.M., 2015. Three Types of Cortical Layer 5 Neurons That Differ in Brain-wide Connectivity and Function. Neuron 88, 1–16.

Kim, H., Hrlund-Richter, S., Wang, X., Deisseroth, K., Carlé, M., Carlé N, M., 2016. Prefrontal Parvalbumin Neurons in Control of Attention. Cell 164, 208–218. doi:10.1016/j.cell.2015.11.038

Komiyama, T., Sato, T.R., O'Connor, D.H., Zhang, Y.-X., Huber, D., Hooks, B.M., Gabitto, M., Svoboda, K., 2010. Learning-related fine-scale specificity imaged in motor cortex circuits of behaving mice. Nature 464, 1182–1186.

Lawrence, P.M., Studholme, K.M., 2014. Retinofugal projections in the mouse. J. Comp. Neurol. 522, 3733–3753. doi:10.1002/cne.23635

Lee, S.-H., Kwan, A.C., Zhang, S., Phoumthipphavong, V., Flannery, J.G., Masmanidis, S.C., Taniguchi, H., Huang, Z.J., Zhang, F., Boyden, E.S., Deisseroth, K., Dan, Y., 2012. Activation of specific interneurons improves V1 feature selectivity and visual perception. Nature 488, 379–383. doi:10.1038/nature11312

Lien, A.D., Scanziani, M., 2013. Tuned thalamic excitation is amplified by visual cortical circuits. Nat. Neurosci. 16, 1315–1323.

Luo, L., Callaway, E.M., Svoboda, K., 2008. Genetic Dissection of Neural Circuits. Neuron 57, 634–660.

Marshel, J.H., Garrett, M.E., Nauhaus, I., Callaway, E.M., 2011. Functional Specialization of Seven Mouse Visual Cortical Areas. Neuron 72, 1040–1054.

Mason, R., 1978. Functional organization in the cat's pulvinar complex. Exp. Brain Res. 31, 51–66.

Movshon, J.A., Adelson, E.H., Gizzi, M.S., Newsome, W.T., 1985. The Analysis of Moving Visual Patterns, in: Chagas, C., Gattass, R., Gross, C. (Eds.), Study Week on Pattern Recognition Mechanisms. Academia Scientiarum Scripta, pp. 118–151.

Movshon, J.A., Newsome, W.T., 1996. Visual response properties of striate cortical neurons projecting to area MT in macaque monkeys. J. Neurosci. 16, 7733–7741.

Muir, D.R., Roth, M.M., Helmchen, F., Kampa, B.M., 2015. Model-based analysis of pattern motion processing in mouse primary visual cortex. Front. Neural Circuits 9, 38.

Newsome, W.T., Paré, E.B., 1988. A selective impairment of motion perception following lesions of the middle temporal visual area (MT). J. Neurosci. 8, 2201–11.

Niell, C.M., 2011. Exploring the next frontier of mouse vision. Neuron 72, 889–892. doi:10.1016/j.neuron.2011.12.011

Niell, C.M., Stryker, M.P., 2008. Highly Selective Receptive Fields in Mouse Visual Cortex. J. Neurosci. 28, 7520–7536.

Nienborg, H., Hasenstaub, A., Nauhaus, I., Taniguchi, H., Huang, Z.J., Callaway, E.M., 2013. Contrast dependence and differential contributions from somatostatin- and parvalbumin-expressing neurons to spatial integration in mouse V1. J. Neurosci. 33, 11145–11154.

Okun, M., Lak, A., Carandini, M., Harris, K.D., 2016. Long term recordings with immobile silicon probes in the mouse cortex. PLoS One 11, e0151180. doi:10.1371/journal.pone.0151180

Olshausen, B.A., Anderson, C.H., Van Essen, D.C., 1993. A neurobiological model of visual attention and invariant pattern recognition based on dynamic routing of information. J. Neurosci. 13, 4700–4719.

Packer, A.M., Russell, L.E., Dalgleish, H.W.P., Häusser, M., 2014. Simultaneous all-optical manipulation and recording of neural circuit activity with cellular resolution in vivo. Nat. Methods 12, 140–146. doi:10.1038/nmeth.3217

Peters, A.J., Chen, S.X., Komiyama, T., 2014. Emergence of reproducible spatiotemporal activity during motor learning. Nature 510, 263–267.

Polack, P.O., Contreras, D., 2012. Long-Range Parallel Processing and Local Recurrent Activity in the Visual Cortex of the Mouse. J. Neurosci. 32, 11120–11131.

Prusky, G.T., West, P.W., Douglas, R.M., 2000. Behavioral assessment of visual acuity in mice and rats. Vision Res. 40, 2201–2209.

Rosa, M.G., Krubitzer, L.A., 1999. The evolution of visual cortex: where is V2? Trends Neurosci. 22, 242–248.

Roth, M.M., Dahmen, J.C., Muir, D.R., Imhof, F., Martini, F.J., Hofer, S.B., 2015. Thalamic nuclei convey diverse contextual information to layer 1 of visual cortex. Nat. Neurosci. 19, 299–307.

Roth, M.M., Helmchen, F., Kampa, B.M., 2012. Distinct functional properties of primary and posteromedial visual area of mouse neocortex. J. Neurosci. 32, 9716–9726.

Rudolph, K., Pasternak, T., 1999. Transient and Permanent Deficits in Motion Perception after Lesions of Cortical Areas MT and MST in the Macaque Monkey. Cereb. Cortex 9, 90–100. doi:10.1093/cercor/9.1.90

Rust, N.C., Mante, V., Simoncelli, E.P., Movshon, J.A., 2006. How MT cells analyze the motion of visual patterns. Nat. Neurosci. 9, 1421–1431.

Sejnowski, T.J., Churchland, P.S., Movshon, J.A., 2014. Putting big data to good use in neuroscience. Nat. Neurosci. 17, 1440–1441.

Shipp, S., 2003. The functional logic of cortico-pulvinar connections. Philos. Trans. R. Soc. Lond. B. Biol. Sci. 358, 1605–1624.

Smith, S.L., Häusser, M., 2010. Parallel processing of visual space by neighboring neurons in mouse visual cortex. Nat. Neurosci. 13, 1144–1149.

Snow, J.C., Allen, H.A., Rafal, R.D., Humphreys, G.W., 2009. Impaired attentional selection following lesions to human pulvinar: evidence for homology between human and monkey. Proc. Natl. Acad. Sci. 106, 4054–4059.

Sohya, K., Kameyama, K., Yanagawa, Y., Obata, K., Tsumoto, T., 2007. GABAergic neurons are less selective to stimulus orientation than excitatory neurons in layer II/III of visual cortex, as revealed by in vivo functional Ca2+ imaging in transgenic mice. J. Neurosci. 27, 2145–2149. doi:10.1523/JNEUROSCI.4641-06.2007

Spencer, K.M., Nestor, P.G., Niznikiewicz, M. a, Salisbury, D.F., Shenton, M.E., McCarley, R.W., 2003. Abnormal neural synchrony in schizophrenia. J. Neurosci. 23, 7407–7411. doi:23/19/7407 [pii]

Stoner, G.R., Albright, T.D., 1992. Neural correlates of perceptual motion coherence. Nature 358, 412–414.

Stoner, G.R., Albright, T.D., Ramachandran, V.S., 1990. Transparency and coherence in human motion perception. Nature 344, 153–155. doi:10.1038/344153a0

Takahashi, T., 1985. The organization of the lateral thalamus of the hooded rat. J. Comp. Neurol. 231, 281–309. doi:10.1002/cne.902310302

Taniguchi, H., He, M., Wu, P., Kim, S., Paik, R., Sugino, K., Kvitsiani, D., Kvitsani, D., Fu, Y., Lu, J., Lin, Y., Miyoshi, G., Shima, Y., Fishell, G., Nelson, S.B., Huang, Z.J., 2011. A resource of Cre driver lines for genetic targeting of GABAergic neurons in cerebral cortex. Neuron 71, 995–1013. doi:10.1016/j.neuron.2011.07.026

Tinsley, C.J., Webb, B.S., Barraclough, N.E., Vincent, C.J., Parker, A., Derrington, A.M., 2003. The nature of V1 neural responses to 2D moving patterns depends on receptive-field structure in the marmoset monkey. J. Neurophysiol. 90, 930–937.

Tohmi, M., Meguro, R., Tsukano, H., Hishida, R., Shibuki, K., 2014. The Extrageniculate Visual Pathway Generates Distinct Response Properties in the Higher Visual Areas of Mice. Curr. Biol. 1–11.

Tsao, D.Y., Freiwald, W.A., Tootell, R.B.H., Livingstone, M.S., 2006. A Cortical Region Consisting Entirely of Face-Selective Cells. Science (80-.). 311, 670–674. doi:10.1126/science.1119983

Ungerleider, L., 1994. “What” and “where” in the human brain. Curr. Opin. Neurobiol. 4, 157–165.

Ungerleider, L.G., Mishkin, M., 1982. Two cortical visual systems [WWW Document]. Anal. Vis. Behav. doi:10.2139/ssrn.1353746

Vandecasteele, M., M., S., Royer, S., Belluscio, M., Berényi, A., Diba, K., Fujisawa, S., Grosmark, A., Mao, D., Mizuseki, K., Patel, J., Stark, E., Sullivan, D., Watson, B., Buzsáki, G., 2012. Large-scale Recording of Neurons by Movable Silicon Probes in Behaving Rodents. J. Vis. Exp. doi:10.3791/3568

Vissers, M.E., X Cohen, M., Geurts, H.M., 2012. Brain connectivity and high functioning autism: A promising path of research that needs refined models, methodological convergence, and stronger behavioral links. Neurosci. Biobehav. Rev. doi:10.1016/j.neubiorev.2011.09.003

Wall, N.R., De La Parra, M., Sorokin, J.M., Taniguchi, H., Huang, Z.J., Callaway, E.M., 2016. Brain-Wide Maps of Synaptic Input to Cortical Interneurons. J. Neurosci. 36, 4000–4009. doi:10.1523/JNEUROSCI.3967-15.2016

Wang, Q., Burkhalter, A., 2007. Area map of mouse visual cortex. J. Comp. Neurol. 502, 339–357. doi:10.1002/cne.21286

Wang, R.Y., White, F.J., Voigt, M.M., 1984. Cholecystokinin, dopamine and schizophrenia. Trends Pharmacol. Sci. 5, 436–438. doi:10.1016/0165-6147(84)90496-6

Wimmer, R.D., Schmitt, L.I., Davidson, T.J., Nakajima, M., Deisseroth, K., Halassa, M.M., 2015. Thalamic control of sensory selection in divided attention. Nature 526, 705–709. doi:10.1038/nature15398

Zhang, X.-Y., Zhou, D.-F., Zhang, P.-Y., Wei, J., 2000. The CCK-A receptor gene possibly associated with positive symptoms of schizophrenia. Mol. Psychiatry 5, 239–240. doi:10.1038/sj.mp.4000677

Zhou, H., Schafer, R.J., Desimone, R., 2016. Pulvinar-Cortex Interactions in Vision and Attention. Neuron 89, 209–220.

Zoccolan, D., Oertelt, N., DiCarlo, J.J., Cox, D.D., 2009. A rodent model for the study of invariant visual object recognition. Proc. Natl. Acad. Sci. 106, 8748–8753.

Chapter 1. Pattern and Component Motion Responses in Mouse Visual Cortex

Summary

Spanning about 9 mm^2 of the posterior cortex surface, the mouse's small but organized visual cortex has recently gained attention for its surprising sophistication and experimental tractability (Carandini and Churchland, 2013; Glickfeld et al., 2014; Hübener, 2003). Though it lacks the highly ordered orientation columns of primates (Ohki et al., 2005), mouse visual cortex is organized retinotopically (Wagor et al., 1980) and contains at least 10 extrastriate areas that likely integrate more complex visual features via dorsal and ventral streams of processing (Andermann et al., 2011; Garrett et al., 2014; Marshel et al., 2011; Polack and Contreras, 2012; Roth et al., 2012; Wang and Burkhalter, 2013; 2007; Wang et al., 2011; 2012). Extending our understanding of visual perception to the mouse model is justified by the evolving ability to interrogate specific neural circuits using genetic and molecular techniques (Callaway, 2005; Luo et al., 2008). In order to probe the functional properties of the putative mouse dorsal stream, we used moving plaids, which demonstrate differences between cells that identify local motion (component cells) and those that integrate global motion of the plaid (pattern cells; Figure 1.1; Movshon et al., 1985). In primates, there are sparse pattern cell responses in primate V1 (Khawaja et al., 2009; Tinsley et al., 2003), but many more in higher-order regions; 25-30% of cells in MT (Movshon et al., 1985) and 40-60% in MST (Khawaja et al., 2013) are pattern direction selective. We present evidence that mice have small numbers of pattern cells in areas LM and RL, while V1, AL, and AM are largely component-like. Although the proportion of pattern cells is smaller in mouse visual cortex than in primate MT,

this study provides evidence that the organization of the mouse visual system shares important similarities to that of primates, and opens the possibility of using mice to probe motion computation mechanisms.

Results

In an effort to extend our understanding of visual information processing in the rodent system so that we may capitalize on experimental advantages, we have used a common stimulus from primate research to probe motion processing in the mouse model. We used intrinsic signal imaging followed by two-photon calcium imaging in layer 2/3 of 2-4 month old anesthetized mice to record responses to grating and plaid stimuli in V1 and four extrastriate areas (LM, AL, RL, and AM).

Although visual areas in the mouse are quite small, borders between areas can be functionally mapped using intrinsic signal optical imaging (Schuett et al., 2002), ideally with a periodic stimulus (Garrett et al., 2014; Kalatsky and Stryker, 2003). We therefore first used intrinsic signal optical imaging during the presentation of a full-field continuous contrasting-reversing checkerboard bar in altitude and azimuth directions to semi-automatically determine borders between visual areas (Figure 1.1; Garrett et al., 2014; Kalatsky and Stryker, 2003; Marshel et al., 2011; Schuett et al., 2002). With this method, functional maps can be accurately computed for each mouse, allowing for individual identification of visual area borders, important due to small area size and slight differences between mice (Garrett et al., 2014). Using these functional maps overlaid on blood vessel patterns as a guide, we then loaded Oregon Green Bapta (OGB) into layer 2/3 of the targeted area (Figure 1.1).

Moving plaids consist of two drifting gratings combined additively and offset by an angle (Figure 1.1; Adelson and Movshon, 1982). In primates, visual area MT/V5 contains cells that respond to the global motion of the plaid, termed “pattern” or “pattern direction selective (PDS)” cells (Figure 1.1; Movshon et al., 1985). Other cells, present in both V1 and MT, encode the individual gratings of the plaid and are termed “component” or “CDS” cells (Figure 1.1). Thus, after OGB loading, we investigated the responses of cells to full screen 100% contrast drifting gratings and 120° plaids (50% contrast for each grating) moving in 12 different directions to identify cells that responded to either the individual, component motions of the plaid or the global, perceived motion of the plaid (Experimental Procedures; Movshon et al., 1985).

We imaged thousands of cells in V1, LM, AL, RL, AM in 34 different animals (Table 1.1). Of these cells, 15-25% (depending on visual area) were responsive ($\Delta F/F > 6\%$) and reliable (determined by a D-prime metric; (Marshel et al., 2011); Supplemental Methods) to at least one type of stimulus [LM: 12.8% (588 out of 4577), AL: 13.4% (508 out of 3970), RL: 17.6% (921 out of 5232), V1: 25% (1192 out of 4743); Table S1], consistent with previous studies investigating visual responses in these areas in both awake (Andermann et al., 2011) and anesthetized (Marshel et al., 2011) mice. Only cells meeting the responsive and reliable criteria for at least one stimulus were included in further analysis to determine stimulus preferences.

We then looked to see whether these cells responded to gratings, plaids, or both. While some cells were responsive and reliable to both stimuli, certain cells responded only to the simple drifting gratings, and another subset responded solely to plaids (Figure 1.2). Across areas, there were differences in the proportions of cells

that were responsive to each stimulus (Figure 1.2); while 38-46% of responsive and reliable cells in V1, LM, AL, and AM responded to both gratings and plaids, 60% (553/921) of cells in RL responded to both. AL had the highest proportion of cells responsive only to gratings (43%; 218/508), while V1 and RL had the lowest (22% and 24%, respectively). A relatively high proportion (37%; 441/1192) of cells in V1 responded exclusively to plaids and not gratings (Figure 1.5).

Only cells that respond to both gratings and plaids can be assessed for their preference for pattern or component motion (Movshon et al., 1985). Furthermore, only direction selective cells can be pattern or component motion direction selective (by the standard definition). Therefore, the subset of cells that were responsive and reliable to both gratings and plaids were then tested for direction selectivity. In V1, about 19.6% of these cells were direction selective (DS; determined by standard metrics where DSI > .5), whereas 22.8-29.2% of cells in LM, AL, and AM were DS, consistent with previous reports (Figure 1.2; (Marshel et al., 2011)). We found a relatively low percentage of DS cells in RL (17.5%), possibly because the stimulus was not optimized for the high-temporal and low-spatial frequency preferences of this area (Marshel et al., 2011). The cells that were responsive and reliable to both gratings and plaids and were also DS were included in the subsequent component/pattern correlation analysis.

In order to characterize cells as pattern, component, or unclassified, we generated predicted tuning curves for pattern and component cells from the grating responses for each cell, as previously described (Figure 1.1; (Movshon et al., 1985)). The two predicted tuning curves were then correlated with the responses to the plaid stimulus to give two correlation values for each cell, Rc and Rp. These correlation

values were then normalized with a Fisher r-to-Z transformation to permit the calculation of a difference between correlation values, generating Z-pattern (Zp) and Z-component (Zc; (Smith et al., 2005)). A significantly high Zp value classifies the cell as pattern-direction selective (PDS), whereas a high Zc value classifies it as component-direction selective (CDS). Cells with correlation values that were not significantly different from each other or zero were deemed unclassified.

Cell responses to the stimulus set of grating and plaids varied on a continuum from PDS to CDS responses. Some cells were CDS and had a very clear bi-lobed tuning curve in response to plaids because a plaid moving in two different directions contained the grating component that the cell preferred (Figure 3B). Alternatively, several cells responded to just one plaid with the same global motion as its preferred grating (Figure 3B), and were therefore PDS.

Across areas, the proportion of PDS, CDS, and unclassified cells differed: LM and RL were the only areas containing cells exhibiting pattern-direction selectivity (Figure 4A). Approximately 5.8% of cells in LM were PDS (4/69), while 8.3% (8/96) of cells in RL were PDS. V1 had no PDS cells but 30.1% (25/83) of the cells included in the analysis (as described above) were classified as CDS. Area AL was marked by the highest percentage of CDS cells (39.5%, 15/38), with many cells that had well-tuned responses to both gratings and plaids. Lastly, AM did not have any PDS cells, but 30.8% (8/26) were clearly CDS. In addition, we conducted a subset of experiments with awake-behaving mice, but this did not drastically change the proportion of pattern cells in RL (Figure S1). Each area had a set of cells that did not significantly correlate with a CDS or PDS prediction, though often these were qualitatively component- or pattern-like (see cell example 2 in Figure 3B).

In addition to cells that are clearly classified as CDS or PDS, the unclassified cells have biases in their responses that can be observed as the difference between Zc and Zp. We therefore also computed a Component Index for each cell by subtracting Zc-Zp to obtain a more graded measure of how the cell responses differed across areas (Figure 4B). The distributions of Zc-Zp values as well as their means differed between the populations of cells sampled in each area with AL being the most component-like and RL the most pattern-like. Specifically, the mean Zc-Zp value was highest (most component-like) for area AL (1.53 +/- 0.22, mean +/- SEM) and was lowest (most pattern-like) for LM (1.05+/-0.18) and RL (0.97+/-0.18). The mean values for areas V1 and AM were intermediate (1.32+/-0.17 and 1.37+/-0.24 respectively).

When proportions of CDS, unclassified, and PDS cells were compared across areas, there were clear significant differences. The number of PDS, unclassified, and CDS was significantly different between V1 and LM ($p<.05$), V1 and RL ($p<.01$), and AL and RL ($p<.05$) as determined by a Fisher Exact Test (Figure 4B; these differences remain significant when corrected for multiple comparisons with a Benjamini-Hochberg procedure, FDR = 0.2). While the number of PDS cells was significantly different in RL and LM when compared to V1, AL and AM were not different from V1 (Figure 4B).

Discussion

While mice have been shown to have multiple visual cortical areas with functional preferences, it is unknown whether these areas generate higher-order functional specializations like those in the primate visual system. In particular, it is

unknown whether mice compute complex visual movement akin to primates. To further assess the potential of mouse visual system for elucidating circuit mechanisms of complex behaviors, we turned to the plaid stimulus, which has proved useful for visual neuroscience in cats and monkeys for the past 30 years (Movshon et al., 1985).

Here we present evidence that mice have cells that can compute pattern motion, and that in the five areas that were tested, these cells are found only in visual areas LM and RL. Meanwhile, mouse V1, AL, and AM do not have any evidence of PDS responses. We found CDS responses in all of the visual areas we tested, suggesting that this is a more fundamental computation that each area can complete. It should be noted that our experiments were restricted to layers 2/3 of cortex, and it is possible that there are laminar differences in responses to plaids. In essence, V1, AL, and AM appear to be “blind” to the global motion of the stimulus, even though many cells in these regions responded in some way to the plaid stimulus. On the contrary, proper processing of moving plaids to provide accurate information about the global movement of the stimulus is effectively completed in specific cells of areas LM and RL, which may constitute a dorsal, movement-sensitive pathway in the mouse (Andermann et al., 2011; Marshel et al., 2011). This integration is essential for correctly computing optic flow and effectively initiating movement.

Although RL contains a much lower percentage of pattern cells than seen in primate MT, it is worth noting that it shares other important similarities with MT. Anatomical studies have suggested that RL is a node of the mouse dorsal stream (Wang et al., 2012). Like MT, RL receives direct input from V1 as well as V2/LM (Wang et al., 2012; 2011), and both MT and RL have a bias towards the lower visual

field in their retinotopic organization (Garrett et al., 2014; Maunsell and Newsome, 1987). RL projects to barrel and whisker motor cortex as well as deep layers of the superior colliculus (Wang and Burkhalter, 2013), suggesting it is involved in navigation and visually-guided orienting. In addition, RL exhibits multisensory enhancement for visual and tactile stimuli (Olcese et al., 2013).

Despite these similarities, there is a marked difference in the direction selectivity of MT and RL – almost every cell in MT is direction selective (Albright, 1984; Dubner and Zeki, 1971) whereas about 18-27% of RL cells are direction selective (Marshel et al., 2011). Shown here, RL is the most pattern-selective area in the mouse, with 8% of direction selective cells responding to pattern motion. While this is a small proportion compared to primate MT, it is unlikely these were recorded by chance in light of the differences between RL and V1. In addition, because the stimulus was not optimized for each individual neuron as in single-cell electrophysiology, it is likely that we have undersampled the number of responsive, and potentially pattern-selective cells. Future studies will need to address the known anatomical and functional markers of MT such as surround suppression, binocular disparity, and direction selective V1 inputs (Born and Bradley, 2005) in order to fully test the validity of the comparison between RL and MT.

Previous studies have shown that mice can compute the global motion of a stimulus, but have not explored the mechanistic basis for this behavior (Douglas et al., 2006). The presence of PDS cells in the mouse suggests that they achieve this computation in a similar way to primates, but with fewer cells overall. It is possible that the downstream consequences of pattern integration, such as motor output for head or body orienting, are achieved with fewer cells that can compute such motion,

or that these computations are completed in networks rather than individual cells. Our observation that many cells respond to plaid stimuli (Figure 2), often in ways that did not conform to a CDS or PDS prediction (Figure 4), suggests that mice might employ a novel computation to perform pattern motion integration and inform downstream behavioral output. This speculation is further supported by the fact that many cells, even in V1, responded significantly to plaids but not gratings (Figure S1). Such cells might support sensation of global motion differently than in primates, obviating the need for large numbers of PDS cells. Alternatively, these cells might prefer spatial frequencies that were present in the plaids but not the gratings.

Evidence for pattern direction selectivity in LM and RL – but not V1, AL, or AM – can build on current anatomical frameworks to inform proper parsing of dorsal and ventral streams in the mouse. While most of the focus has been on pattern selectivity, we are intrigued by the high proportion of component cells in AL. Previous studies have suggested that AL is a gateway to the dorsal stream (Marshel et al., 2011; Wang et al., 2011), yet the present work suggests that it is not involved in plaid motion integration, a prominent characteristic of dorsal stream function. On the other hand, anatomical data has led other researchers to position LM as part of the ventral stream (Wang et al., 2012; 2011), although it clearly projects to both dorsal and ventral targets. Indeed, the rationale used to place LM in the ventral stream places V1 there as well (Wang et al., 2012). Our past investigation into the spatial and temporal frequency preferences of LM (Marshel et al., 2011) and present data for plaid motion processing suggests that LM is involved in the dorsal stream as well, and may be akin to primate V2 in this regard (Kalatsky and Stryker, 2003; Rosa and Krubitzer, 1999). Further functional studies of these areas with more diverse and complex visual

stimuli – including objects, figure/ground separation, colors, etc. – will be necessary to explicate functional differences and draw a clear hierarchy between these regions.

As there is a significant gain in response intensity with movement (Fu et al., 2014; Niell and Stryker, 2010), and other researchers have posited that plaid motion integration may change with brain state ((Pack et al., 2001), but see (Movshon et al., 2003)), we ran a subset of experiments in awake animals but did not see a striking difference in the proportion of pattern cells (Figure S1). Although preliminary, this suggests that plaid motion integration does not depend on the state of the animal (Movshon et al., 2003).

Our work here provides a basis to test the nuances of complex motion perception in mammalian visual systems and further unravels the function of higher-order mouse cortex. The demonstration of pattern motion selective cells in genetically tractable mice, where specific cell types can be selectively manipulated (Luo et al., 2008), opens the door to studies probing the neural circuit mechanisms that underlie the production of pattern motion cells in higher-order visual areas from their component motion selective V1 inputs. The use of single-cell monosynaptic tracing with the rabies virus (Marshel et al., 2010; Wickersham et al., 2007) in conjunction with genetically-encoded calcium indicators could be a fruitful way to understand which cells provide inputs to pattern cells, and how and when these inputs are combined (Movshon and Newsome, 1996; Thiele and Stoner, 2003). Already, various groups have capitalized on the methodological advantages afforded by the mouse model to address circuit-level questions of visual perception (Cruz-Martín et al., 2015; Lien and Scanziani, 2013; Nienborg et al., 2013) – our work provides a necessary basis for similar future studies. The presence of pattern cells in mouse visual cortex

suggests that questions regarding the cell types and connectivity motifs that underlie pattern motion computation can indeed be investigated in the mouse model.

Experimental Procedures

Animal procedures. Experiments were performed on adult (2-4 month) C57/BL6 mice (male and female) under isoflurane anesthesia (0.5-1.2%) with chlorprothexine (10 mg/kg) as a sedative during visual stimulation. Carpofen (5 mg/kg) was administered subcutaneously prior to surgery, and ibuprofen (30 mg/kg) was given in drinking water for one week following. Custom circular head frames were mounted to the skull with dental acrylic. Eyes were kept moist with ointment during surgeries, and covered with a thin layer of silicone oil during visual stimulation. All experiments were approved by the Salk Institute's Institutional Animal Care and Use Committee.

Intrinsic signal optical imaging. The skull was thinned and covered with 1.5% agarose and a coverslip. The stimulus was a full-field continuous contrast-reversing checkerboard bar in both azimuth and altitude directions (Marshel et al., 2011). Absolute retinotopy was computed from phase maps of the response using the difference of the hemodynamic delays for opposing directions of the same orientation. Each trial was 183 seconds, with 10 drifts of the bar across the 55-inch LED screen. The stimulus was spherically corrected to account for distortions in size and spatial frequency that occur when projecting a sphere onto a flat screen. We used an automated program to identify visual area borders based on their field sign maps (Sereno et al., 1994; Garrett et al., 2014) and overlaid those borders with blood vessel pictures to accurately target calcium dye loading (Figure 1.1).

Two-photon calcium imaging. 1-3 days after intrinsic imaging, a 5-6 mm diameter craniotomy was made over the targeted region and calcium indicator Oregon Green 488 Bapta-1 AM (Life Technologies) and astrocyte marker Sulfurhodamine (SR101; Nimmerjahn et al., 2004) were loaded 125-225 μm beneath the pia. Dye was loaded into the center of the targeted visual area and this was confirmed with the retinotopic stimulus during two-photon imaging. The craniotomy was covered with 1.5% agarose and a coverslip, gently applying pressure to brain. Occasionally, a duratomy was also performed prior to securing the coverslip. Scan parameters were 256x256 lines/frame at 2 ms/line. Mice were positioned 13 cm from the screen, which was centered on their eye and pointed towards their nose at a 30° angle.

Two-photon stimuli. Individual gratings were 100% contrast sine waves. Plaid gratings were each 50% contrast sine waves; therefore with the addition of these gratings, the plaids were also 100% contrast. Plaids consisted of two gratings that were 120° (majority of experiments) or 90° (subset of experiments in LM; Figure S1B, black line); data shown in main figures were with 120° plaids. Stimuli were 4 sec and shown in 12 different directions, with a SF of .04 or .025 cycles/deg, and TF of 1, 1.5, or 2 Hz. Each stimulus was repeated 5-8 times, and responses were averaged across these repeats to calculate a mean time course. Each area was shown a combination of SF and TF, biased towards optimal parameters for the individual areas (Marshel et al., 2011). Typically, fields of view were imaged once with one combination of SF and TF. If fields of view were imaged multiple times, only the field of view with the most responsive cells was used in further analysis. Akin to intrinsic imaging, the stimulus was spherically corrected to account for distortions in size and spatial frequency at

the periphery. Stimuli were presented full-screen. Prior to the presentation of gratings and plaids, a drifting checkerboard bar (akin to intrinsic imaging experiments) to ensure that imaging was occurring in the center of visual space (< 60 deg). Both intrinsic signal and two-photon stimuli were generated by a customized PsychToolbox interface, and data acquisition was controlled by a modified version of ScanImage 3.8 (www.scanimage.org).

Preprocessing of calcium data. Regions of interest (ROIs) around each cell were created using a semi-automatic procedure, separately for the OGB channel (neurons and glia) and the sulfarhodamine-101 channel (glia; Figure 1.3, though these fields of view have notably few glial cells). Glial cells were removed from the analysis of the OGB channel by removing any ROIs in the OGB channel that overlapped with ROIs in the SR-101 channel, leaving only neurons for further analysis. To account for drifts in the image over time, we applied a movement correction algorithm that aligned each trial of the experiment to the average image of the first trial by determining the highest cross-correlation between images. Baseline fluorescence (FB) was averaged within each cell ROI for each trial during a 2 sec prestimulus period during which a gray screen was presented. The stimulus-evoked time course was converted from absolute to relative fluorescence by computing $\Delta F/F = (F_I-F_B)/F_B$, where F_I is the instantaneous, stimulus-evoked fluorescence signal over the last 3 sec of the stimulus. This ensured averaging of peak signal and avoidance of averaging over preliminary cell responses, which often have different tuning properties in response to plaids (Smith et al., 2005).

Identification of responsive, reliable, and direction-selective cells. Further analysis was restricted to cells that were responsive ($\Delta F/F > 6\%$) and reliable to both grating and plaid stimuli, as determined by a response reliability metric (δ),

$$\delta = (\mu_{max}-\mu_{blank})/(\sigma_{max}+\sigma_{blank})$$

where μ_{max} and σ_{max} are the mean and standard deviation of the response to the preferred direction for 5-8 repeats of the stimulus and μ_{blank} and σ_{blank} are the mean and standard deviation of the response during blank trials (also 5-8 repeats). This metric has been shown to be an effective way to exclude cells with noisy, unreliable responses (Marshel et al., 2001). A direction selectivity index (DSI) was also computed for each cell, defined as

$$DSI = (\mu_{max}-\mu_{opp})/(\mu_{max}+\mu_{opp})$$

where μmax is the mean response to the preferred direction and μopp is the mean response to the opposite direction (Marshel et al., 2011; Andermann et al., 2011). Cells with a DSI > 0.5 were considered direction-selective and were included in the pattern/component analysis.

Awake behaving OGB experiments. For awake experiments, headframing was done with C&B Metabond Dental Cement ® for more stable structural support. Animals were trained for two sessions (1 hour each) on a vertical running wheel (Personal communication, T. Sato), on which they became proficient at walking/running. OGB was loaded as described above. Thirty minutes after loading, the mouse was allowed to fully wake up (~1.5 hours post loading). Imaging was performed while the mouse was stationary or moving on the wheel, though the mice spent almost all of their time sitting still. Additional movement correction algorithms (StackReg and Template Matching plugins in ImageJ) were applied to correct for

movement. Stimuli during awake experiments were identical, although the screen was positioned at 20-22 cm from the mouse due to the base of the vertical wheel.

Classification of component and pattern cells. After using the responses to the grating to identify reliable and responsive direction-selective cells, we generated predictions for pattern and component cell tuning curves as previously described (Smith et al., 2005; Movshon et al., 1985). These predictions were then compared with the actual plaid tuning curves using the partial correlation equation:

$$R_p = \frac{(r_p - r_c r_{pc})}{\sqrt{(1 - r_c^2)(1 - r_p^2)}}$$

r_p = raw correlation of the data with the pattern prediction

r_c =raw correlation with the component prediction

r_{pc} = correlation between the two predictions

R_p and R_c values for each cell were then transformed with a Fisher's r-to-Z transformation to stabilize the variance (Smith et al., 2005). Each value of Z_p and $Z_c$was then tested for significance: if Z_p exceeded Z_c (or zero, if Z_c is negative) by 1.28 ($p > 0.01$), the cell was deemed a pattern cell, and the reverse was used to classify component cells. Cells with Z_p and Z_c values that were not significantly different were termed unclassified. For each cell, we subtracted Z_c-Z_p to obtain a Component Index. As prior studies have almost exclusively used this classification paradigm with spike rates, it is imperative to consider the potential nonlinearities in the calcium signal. However, previous studies have shown that OGB is linear with the low spike rates as seen in anesthetized mice (Kerlin et al., 2010; Nauhaus et al., 2012).

Figures and Tables

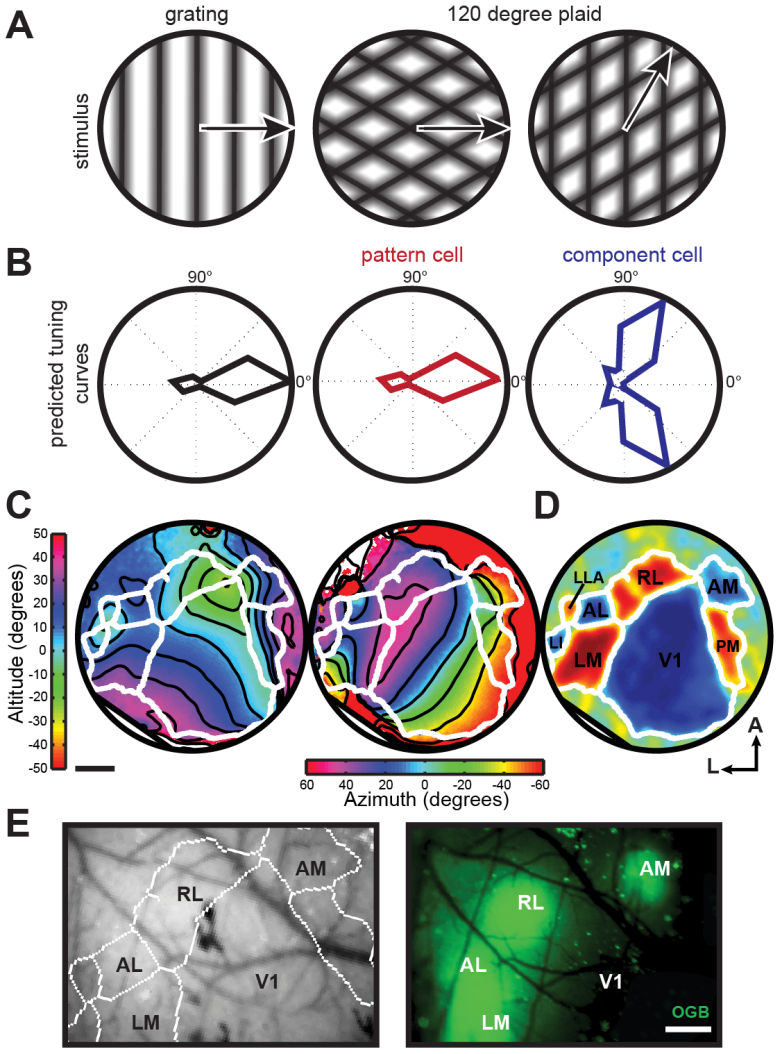

Figure 1.1. Classifying pattern and component-like responses to plaid stimuli in multiple visual areas. (A) Schematic of sinusoidal gratings and plaids. Left plaid has same pattern motion as grating, right plaid has a different pattern motion but contains the rightward-moving grating component. (B) Left - hypothetical response to grating, center and right - generated predictions for pattern and component tuning curves in response to plaids. The pattern response is identical to the DS cell response to the grating, whereas the component response has two lobes to account for the two directions of the plaid (one direction shown in (A)) that contain the preferred component. (C) Sample azimuth and altitude ISI data from one animal with 5 repeats of the stimulus. Contour lines are overlaid in black, area borders as determined by semi-automatic border analysis are overlaid in white. (D) Visual field sign computed as the sine of the difference in the angle between the horizontal and vertical map gradients. Regions with a red visual field sign have a non-mirror representation of visual space, whereas areas in blue have a mirror representation. Regions that are not clearly red or blue lack retinotopic structure. Identified visual areas are labeled. (E) Left - visual area borders generated from (C and D) overlaid on blood vessel picture. Right - subsequent OGB loading into targeted areas. Scale bar represents 500 μm.

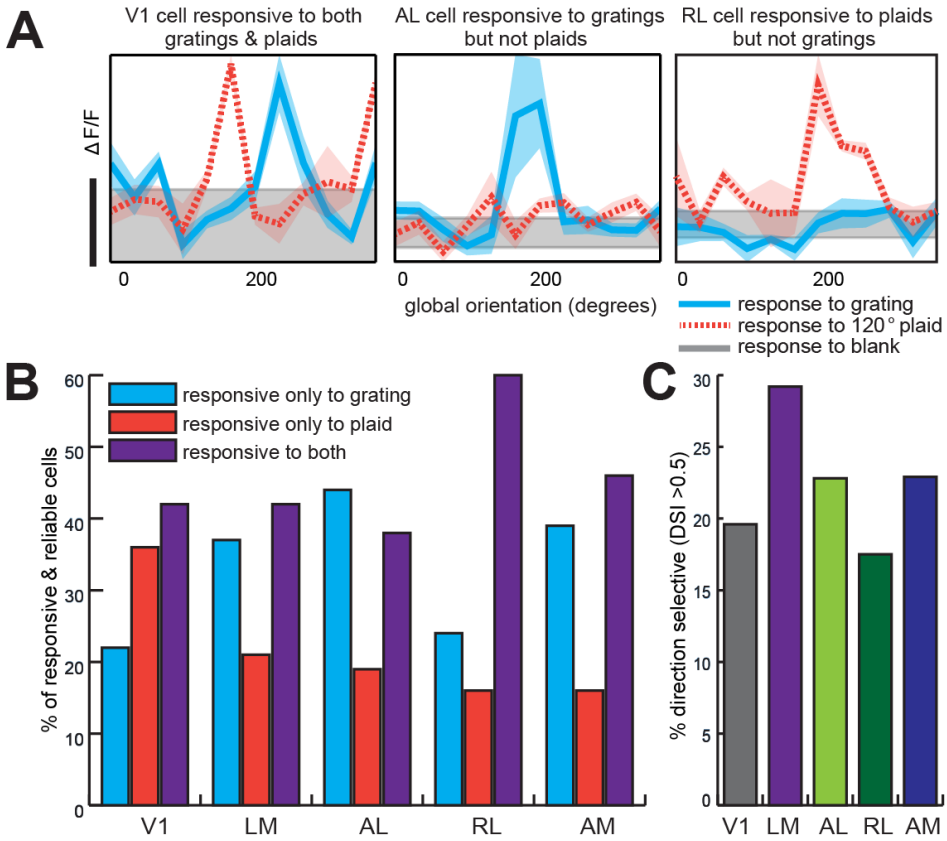

Figure 1.2. Sample tuning curves and distribution of responses to gratings and plaids. (A) Example tuning curves from V1, AL, and RL, demonstrating diverse visual responses to grating or plaid stimuli. Left - V1 cell responds above baseline (gray) to both gratings (cyan) and plaids (orange dashed line), center - AL cell responds to only gratings, and right - RL cell responds only to plaids. Shaded area around curves represents S.E.M; gray baseline shaded area is the mean ΔF/F +/- S.E.M. Scale bar corresponds to 5% ΔF/F. (B) Percent of responsive and reliable cells in each area that responded to only drifting gratings, only 120° plaids, or both. (C) Percent of cells that were direction selective (DSI>0.5), taken out of the total number of responsive & reliable cells. See also Figure S1.

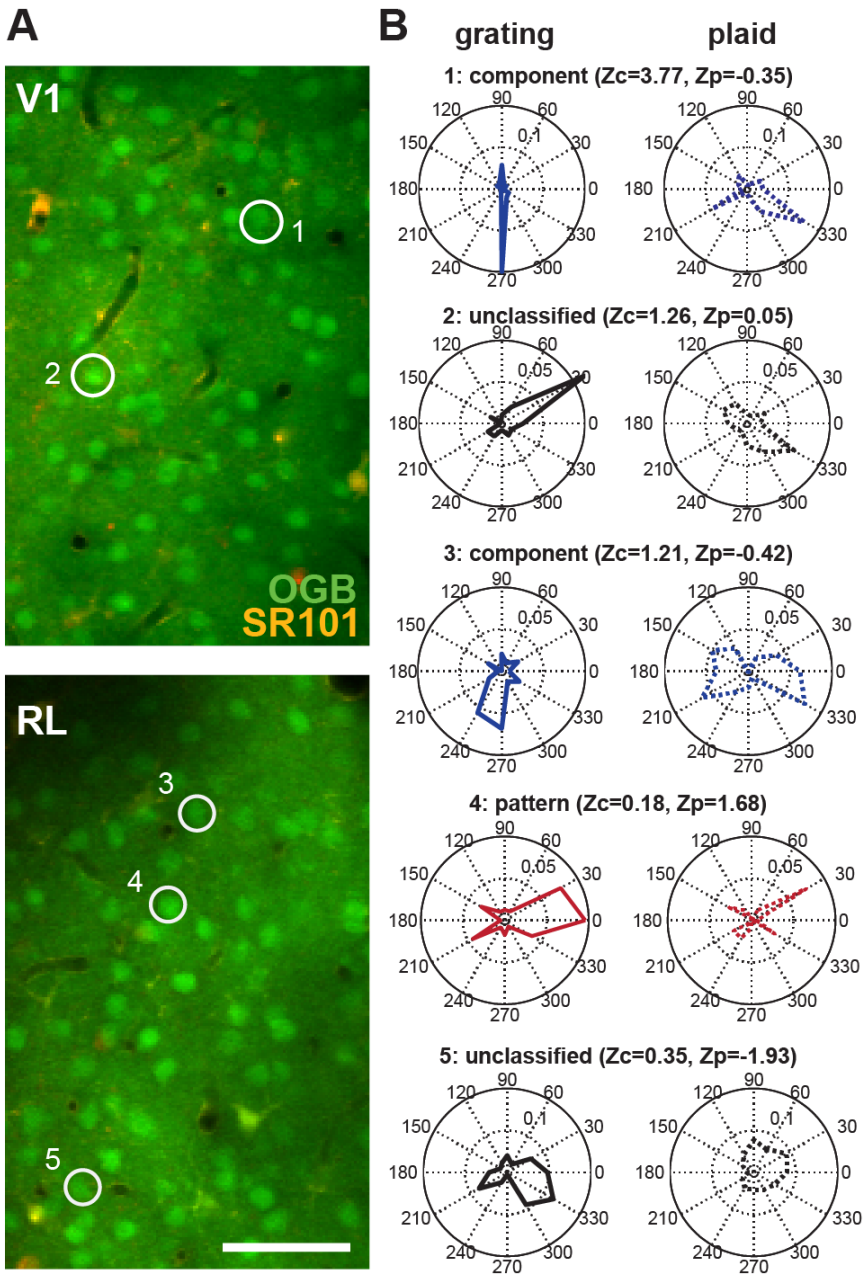

Figure 1.3. OGB and SR101 loading in V1 and RL with cell examples. (A) Example two-photon data from V1 (top) and RL (bottom) with OGB (neurons) and SR101 (glia) loading. Scale bar represents 50 μm. (B) Sample tuning curves from component, unclassified, and pattern cells. Z-scored component (Zc) and pattern (Zp) values are given for each cell. Numbered circles in the images (A) indicate neurons that correspond to the numbered tuning curves (B). Values within polar plots indicate ΔF/F scale to the inner dotted ring of each plot.

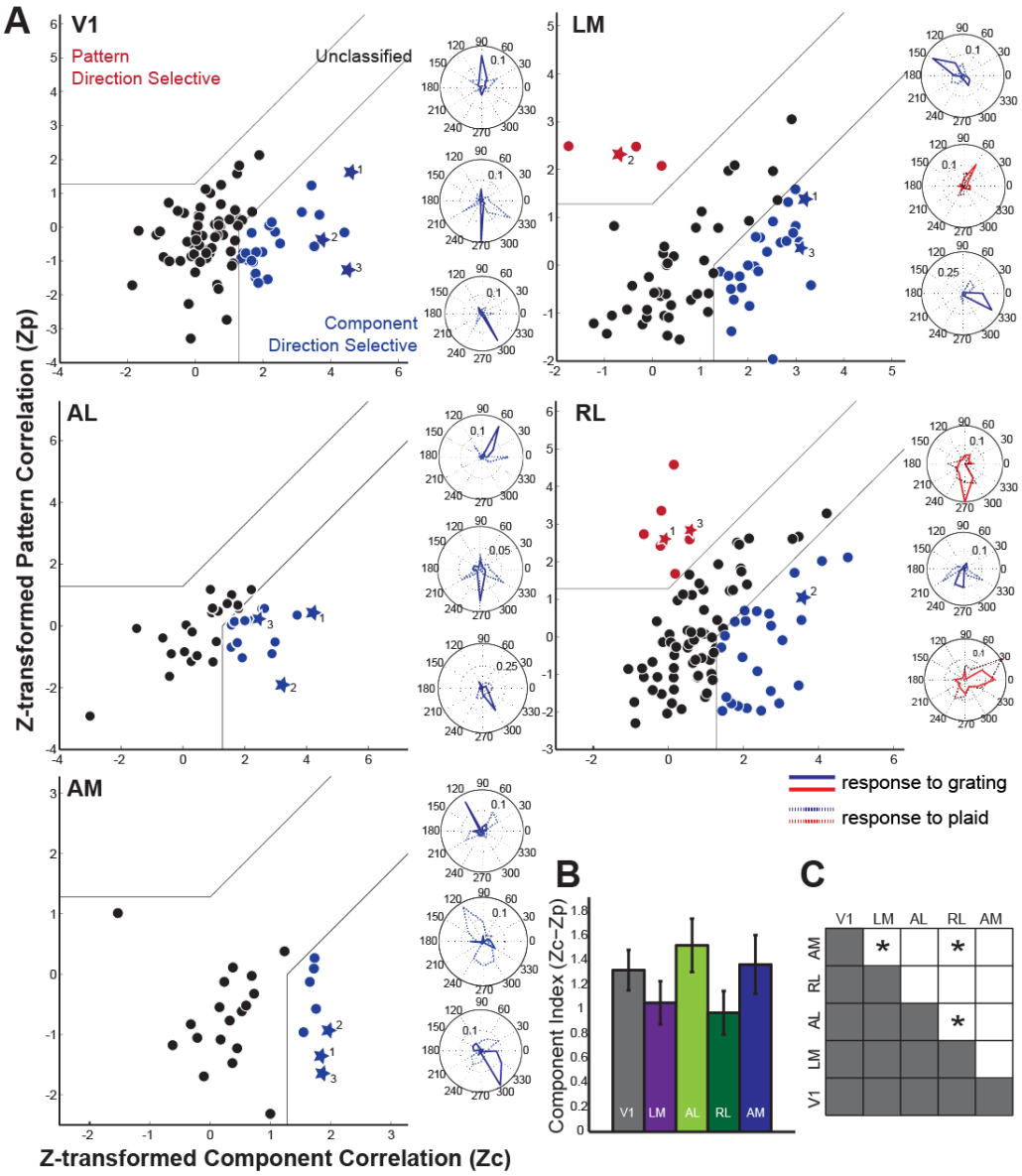

Figure 1.4. Pattern and component correlation plots by visual area. (A) Z-transformed pattern (Zp) vs. component (Zc) correlation for V1, LM, AL, RL, and AM. Cells with tuning curves plotted to the right are denoted as stars in the scatterplots. All cells are colored according to classification (red-pattern, black-unclassified, blue-component). Gray lines divide plots into areas of significantly Pattern Direction Selective (PDS), unclassified, or Component Direction Selective (CDS). Outside ring of polar plots is color coded for each visual area. Values within polar plots indicate ΔF/F scale to the inner dotted ring of each plot; inner ring is 10% ΔF/F unless otherwise noted. (B) Mean component index (Zc-Zp) by visual area, error bars show S.E.M. *p < .05 (Fisher Exact Test). (C) Top – schematic of mouse visual areas. Bottom -Average Zc score plotted against the average Zp score for each visual area, error bars show S.E.M. The visual area corresponding to each point is indicated by colors in top area schematic. For further characterization of this data, see Figure 1.6.

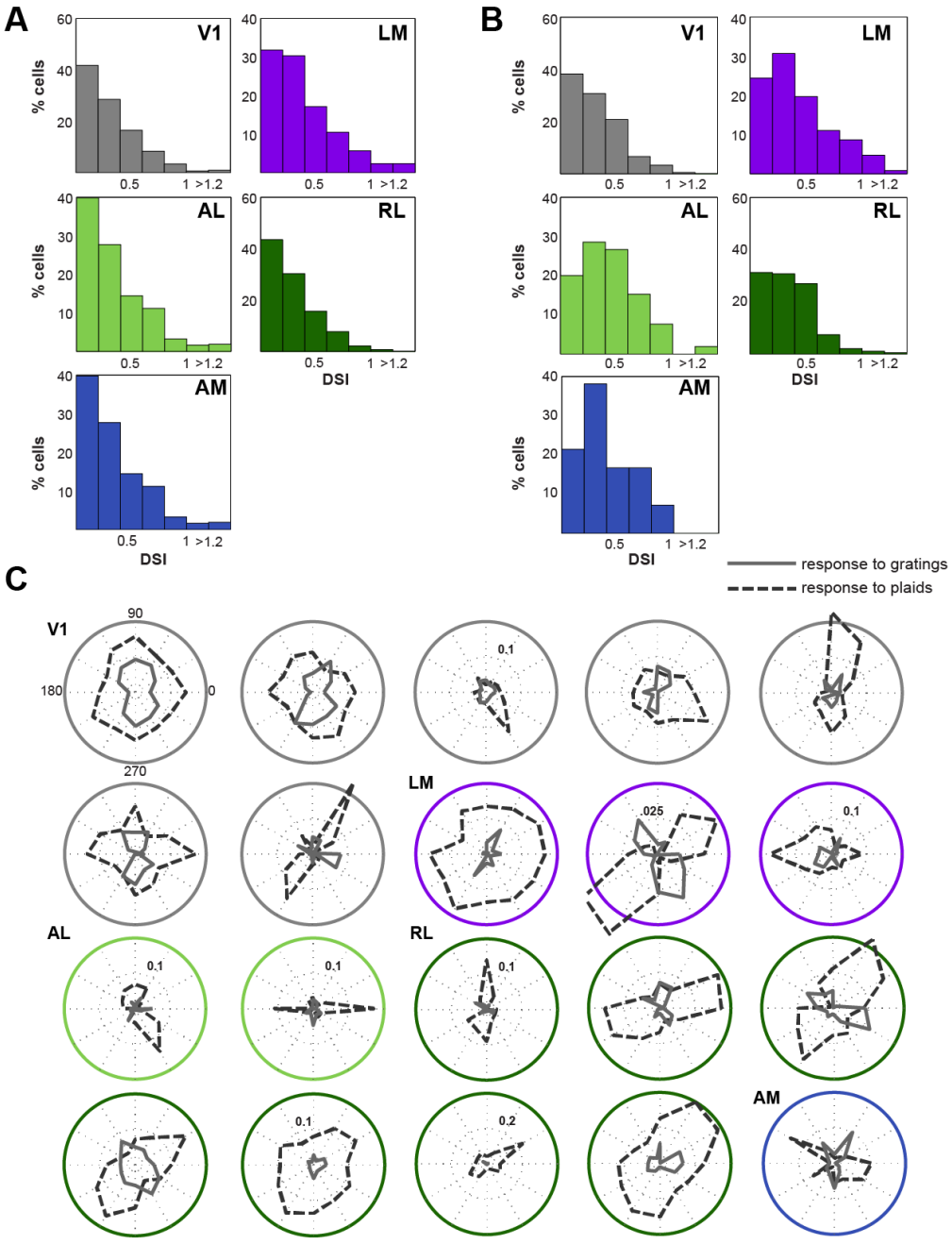

Figure 1.5. Direction selectivity and sample responses to plaids but not gratings. (A) Histograms of DSI selectivity for all responsive and reliable cells in each visual area. Values reflect percentages of responsive and reliable cells. (B) Histograms of DSI in response to plaids for all cells that responded exclusively to plaids (but not gratings). Values reflect percentages of responsive and reliable cells. (C) Polar plots for example cells that responded to plaids but not gratings. Many cells demonstrate bi-directional tuning to plaids, others responded broadly to plaids. Outside ring of polar plots is color coded for each visual area. Values within polar plots indicate ΔF/F scale to the inner dotted ring of each plot; inner ring is 5% ΔF/F unless otherwise noted. Responses to gratings are solid lines; plaids are dashed lines.

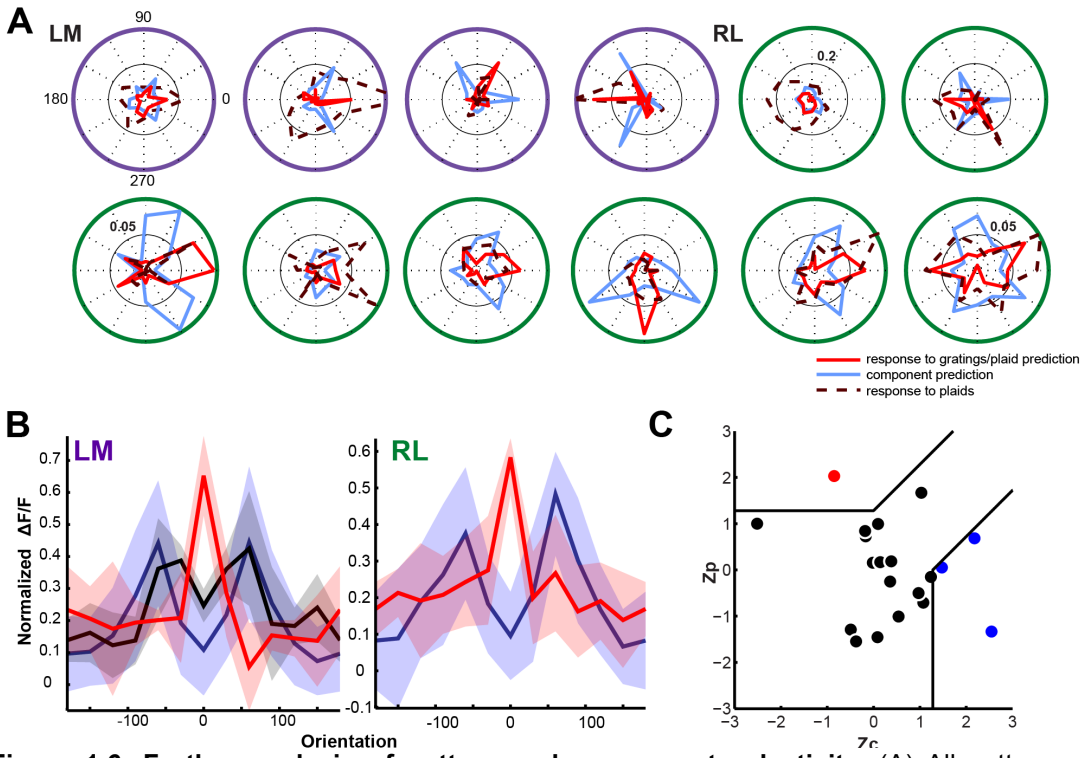

Figure 1.6. Further analysis of pattern and component selectivity. (A) All pattern cell tuning curves. PDS cells were found in LM and RL. Solid red tuning curves are in response to drifting gratings, dashed dark red tuning curves are in response to plaids, light blue lines are component predictions. Values within polar plots indicate ΔF/F scale to the inner dotted ring of each plot; inner ring is 10% ΔF/F unless otherwise noted. (B) Overlay of normalized tuning curves in response to 90° and 120° plaids for LM (left) and RL (right). Tuning curves for PDS and CDS cells within LM or RL were normalized, centered, and then averaged to generate an average tuning curve for each cell classification: PDS cells (red), CDS cells at 90° plaids (black, when data was available), and CDS cells at 120° plaids (blue). Shaded regions indicate S.E.M. (C) Z-scored component and pattern correlation plot for awake-behaving RL experiments (3 animals, n = 20). (D) Plaid indices for cells in area RL (n=96; same cells in Figure 4) plotted against D-Prime (top) and Response Magnitude (bottom). Left - Pattern correlation scores (Zp). Center - Component correlation scores (Zc). Right - Component index (Zc-Zp). (E) Zp scores plotted against DSI values, for each visual area. Vertical dotted line denotes DSI criterion of 0.5 for plaid analysis. Cells with DSI values greater than 1.5 have been placed in last bin (DSI = 1.5). (F) Characterization of responses to plaids in cells with bi-directional tuning. The population of responsive and reliable cells was restricted to cells with OSI > 0.5, without a DSI restriction, and pattern/component correlations were calculated as previously described and displayed as in Figure 4. Cells with tuning curves plotted to the right are denoted as stars in the scatterplots. All cells are colored according to classification (red-pattern, black-unclassified, blue-component). Gray lines divide plots into areas of significantly Pattern Direction Selective (PDS), unclassified, or Component Direction Selective (CDS). Values within polar plots indicate ΔF/F scale to the inner dotted ring of each plot; inner ring is 5% ΔF/F unless otherwise noted. Overall, more cells were included in these analyses, as more cells met the OSI > 0.5 criteria. In V1, LM, RL, and AM, additional bi-directional pattern cells were identified. (G) Mean Component Index by area; error bars show S.E.M. Means were significantly different as tested with a one-way ANOVA (p=.0007). (H) Significant differences between proportions of PDS, unclassified, and CDS cells (*p < .05; as tested with a chi-square contingency table).

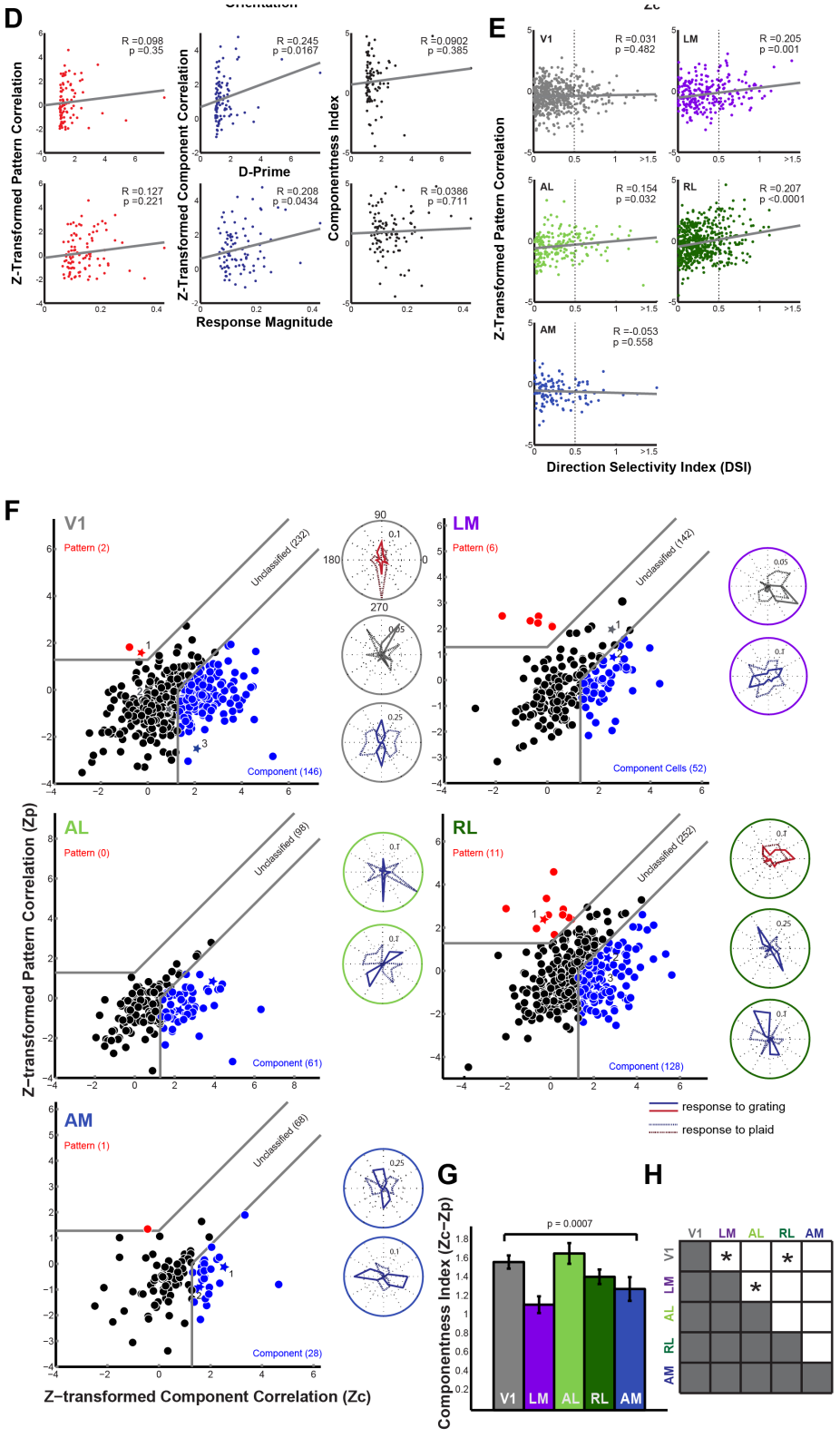

Figure 1.6. Further analysis of pattern and component selectivity (continued).

Table 1.1 Summary of Experiments. Fields of view represent individual experiments, often in the same animal. Percentages reflect proportion of total number of cells sampled. Shaded region includes cells that were responsive and reliable to both grating and plaid stimuli as well as direction selective, and were therefore included in subsequent analyses to determine component and pattern selectivity. Anim: animals; R&R: Responsive & Reliable; DSI: Direction Selectivity Index; CDS: Component Direction Selective; PDS: Pattern Direction Selective.

Area	Anim	Fields of View	Total # of Cells Sampled	Responsive & Reliable (to gratings and/or plaids)	R&R to Gratings (a)	R&R to Plaids (b)	R&R to Gratings and Plaids (c)	Included in Plaid Analysis (cells in (c) with DSI>0.5)	CDS Cells	PDS Cells
V1	9	18	4743	1192(25.1%)	749(15.8%)	903(19.0%)	489(10.3%)	83(1.7%)	25	0
LM	8	26	4577	588(12.8%)	466(10.2%)	369(8.1%)	247(5.4%)	69(1.5%)	26	4
AL	7	18	3790	508(13.4%)	414(10.9%)	284(7.5%)	190(5.0%)	38(1.0%)	16	0
RL	10	26	5232	921(17.6%)	772(14.8%)	702(13.4%)	553(10.6%)	96(1.8%)	25	8
AM	8	12	1818	264(14.5%)	223(12.3%)	162(8.9%)	121(6.7%)	26(1.4%)	8	0
Awake-behaving experiments:										
RL	3	8	1188	92(7.7%)	78(6.6%)	74(6.2%)	60(5.1%)	20(1.7%)	3	1

Acknowledgements

We wish to thank Drs. Tony Movshon and Marina Garrett for insightful feedback on the experimental design and manuscript, Drs. Jim Marshel and Ian Nauhaus for MATLAB assistance, as well as the Callaway lab members for helpful discussions. This work was supported by the NIH (EY022577) and the Gatsby Charitable Foundation (E.M.C.), and the NSF and Martinet Foundation (A.L.J.). The authors declare no conflict of interest.

Chapter 1, in full, is a reprint of the material as it appears in Juavinett, A.L. & Callaway, E.M. (2015) *Current Biology* 25(13): 1759-64. The dissertation author was the primary author of this paper.

References

Adelson, E.H., Movshon, J.A., 1982. Phenomenal coherence of moving visual patterns. Nature 300, 523–525.

Albright, T.D., 1984. Direction and orientation selectivity of neurons in visual area MT of the macaque. Journal of Neurophysiology 52, 1106–1130.

Andermann, M.L., Kerlin, A.M., Roumis, D.K., Glickfeld, L.L., Reid, R.C., 2011. Functional Specialization of Mouse Higher Visual Cortical Areas. Neuron 72, 1025–1039. doi:10.1016/j.neuron.2011.11.013

Born, R.T., Bradley, D.C., 2005. Structure and function of visual area MT. Annu. Rev. Neurosci. 28, 157–189. doi:10.1146/annurev.neuro.26.041002.131052

Callaway, E.M., 2005. A molecular and genetic arsenal for systems neuroscience. Trends in Neurosciences 28, 196–201. doi:10.1016/j.tins.2005.01.007

Carandini, M., Churchland, A.K., 2013. Probing perceptual decisions in rodents. Nat Neurosci 16, 824–831. doi:10.1038/nn.3410

Cruz-Martín, A., El-Danaf, R.N., Osakada, F., Sriram, B., Dhande, O.S., Nguyen, P.L., Callaway, E.M., Ghosh, A., Huberman, A.D., 2015. A dedicated circuit links direction-selective retinal ganglion cells to the primary visual cortex. Nature 507, 358–361. doi:10.1038/nature12989

Douglas, R.M., Neve, A., Quittenbaum, J.P., Alam, N.M., Prusky, G.T., 2006. Perception of visual motion coherence by rats and mice. Vision Research 46, 2842–2847. doi:10.1016/j.visres.2006.02.025

Dubner, R., Zeki, S.M., 1971. Response properties and receptive fields of cells in an anatomically defined region of the superior temporal sulcus in the monkey. Brain Research 35, 528–532.

Fu, Y., Tucciarone, J.M., Espinosa, J.S., Sheng, N., Darcy, D.P., Nicoll, R.A., Huang, Z.J., Stryker, M.P., 2014. A Cortical Circuit for Gain Control by Behavioral State. Cell 156, 1139–1152. doi:10.1016/j.cell.2014.01.050

Garrett, M.E., Nauhaus, I., Marshel, J.H., Callaway, E.M., 2014. Topography and areal organization of mouse visual cortex. Journal of Neuroscience 34, 12587–12600. doi:10.1523/JNEUROSCI.1124-14.2014

Glickfeld, L.L., Reid, R.C., Andermann, M.L., 2014. A mouse model of higher visual cortical function. Current Opinion in Neurobiology 24, 28–33. doi:10.1016/j.conb.2013.08.009

Hübener, M., 2003. Mouse visual cortex. Current Opinion in Neurobiology 13, 413–420. doi:10.1016/S0959-4388(03)00102-8

Kalatsky, V.A., Stryker, M.P., 2003. New paradigm for optical imaging: temporally encoded maps of intrinsic signal. Neuron 38, 529–545.

Kerlin, A.M., Andermann, M.L., Berezovskii, V.K., Reid, R.C., 2010. Broadly tuned response properties of diverse inhibitory neuron subtypes in mouse visual cortex. Neuron 67, 858–871.

Khawaja, F.A., Liu, L.D., Pack, C.C., 2013. Responses of MST neurons to plaid stimuli. Journal of Neurophysiology 110, 63–74. doi:10.1152/jn.00338.2012

Khawaja, F.A., Tsui, J.M.G., Pack, C.C., 2009. Pattern Motion Selectivity of Spiking Outputs and Local Field Potentials in Macaque Visual Cortex. Journal of Neuroscience 29, 13702–13709. doi:10.1523/JNEUROSCI.2844-09.2009

Lien, A.D., Scanziani, M., 2013. Tuned thalamic excitation is amplified by visual cortical circuits. Nat Neurosci 16, 1315–1323. doi:10.1038/nn.3488

Luo, L., Callaway, E.M., Svoboda, K., 2008. Genetic Dissection of Neural Circuits. Neuron 57, 634–660. doi:10.1016/j.neuron.2008.01.002

Marshel, J.H., Garrett, M.E., Nauhaus, I., Callaway, E.M., 2011. Functional Specialization of Seven Mouse Visual Cortical Areas. Neuron 72, 1040–1054. doi:10.1016/j.neuron.2011.12.004

Marshel, J.H., Mori, T., Nielsen, K.J., Callaway, E.M., 2010. Targeting single neuronal networks for gene expression and cell labeling in vivo. Neuron 67, 562–574.

Maunsell, J.H., Newsome, W.T., 1987. Visual processing in monkey extrastriate cortex. Annu. Rev. Neurosci. 10, 363–401.

Movshon, J.A., Adelson, E.H., Gizzi, M.S., Newsome, W.T., 1985. The Analysis of Moving Visual Patterns, in Pattern Recognition Mechanisms, eds. Chagas, C., Gattass, R. & Gross, C. Academia Scientiarum Scripta.

Movshon, J.A., Albright, T.D., Stoner, G.R., Majaj, N.J., 2003. Cortical responses to visual motion in alert and anesthetized monkeys. Nature.

Movshon, J.A., Newsome, W.T., 1996. Visual response properties of striate cortical neurons projecting to area MT in macaque monkeys. J. Neurosci. 16, 7733–7741.

Nauhaus, I., Nielsen, K.J., Callaway, E.M., 2012. Nonlinearity of two-photon Ca2+ imaging yields distorted measurements of tuning for V1 neuronal populations. J. Neurophysiol. 107, 923–936.

Niell, C.M., Stryker, M.P., 2010. Modulation of Visual Responses by Behavioral State in Mouse Visual Cortex. Neuron 65, 472–479.

Nienborg, H., Hasenstaub, A., Nauhaus, I., Taniguchi, H., Huang, Z.J., Callaway, E.M., 2013. Contrast dependence and differential contributions from somatostatin- and parvalbumin-expressing neurons to spatial integration in mouse V1. J. Neurosci. 33, 11145–11154.

Nimmerjahn, A., Kirchhoff, F., Kerr, J.N.D., Helmchen, F., 2004. Sulforhodamine 101 as a specific marker of astroglia in the neocortex in vivo. Nat. Methods 1, 31–37.

Ohki, K., Chung, S., Ch'ng, Y.H., Kara, P., Reid, R.C., 2005. Functional imaging with cellular resolution reveals precise micro-architecture in visual cortex. Nature 433, 597–603.

Olcese, U., Iurilli, G., Medini, P., 2013. Cellular and Synaptic Architecture of Multisensory Integration in the Mouse Neocortex. Neuron 1–15.

Pack, C.C., Berezovskii, V.K., Born, R.T., 2001. Dynamic properties of neurons in cortical area MT in alert and anaesthetized macaque monkeys. Nature 414, 905–908.

Polack, P.O., Contreras, D., 2012. Long-Range Parallel Processing and Local Recurrent Activity in the Visual Cortex of the Mouse. J. Neurosci. 32, 11120–11131.

Rosa, M.G., Krubitzer, L.A., 1999. The evolution of visual cortex: where is V2? Trends in Neurosciences 22, 242–248.

Roth, M.M., Helmchen, F., Kampa, B.M., 2012. Distinct Functional Properties of Primary and Posteromedial Visual Area of Mouse Neocortex. J. Neurosci. 32, 9716–9726.

Sereno, M.I., McDonald, C.T., Allman, J.M., 1994. Analysis of retinotopic maps in extrastriate cortex. Cereb. Cortex 4, 601–620.

Schuett, S., Bonhoeffer, T., Hübener, M., 2002. Mapping retinotopic structure in mouse visual cortex with optical imaging. Journal of Neuroscience 22, 6549–6559.

Smith, M.A., Majaj, N.J., Movshon, J.A., 2005. Dynamics of motion signaling by neurons in macaque area MT. Nat Neurosci 8, 220–228. doi:10.1038/nn1382

Thiele, A., Stoner, G., 2003. Neuronal synchrony does not correlate with motion coherence in cortical area MT. Nature 421, 366–370. doi:10.1038/nature01285

Tinsley, C.J., Webb, B.S., Barraclough, N.E., Vincent, C.J., Parker, A., Derrington, A.M., 2003. The nature of V1 neural responses to 2D moving patterns depends on receptive-field structure in the marmoset monkey. Journal of Neurophysiology 90, 930–937. doi:10.1152/jn.00708.2002

Wagor, E., Mangini, N.J., Pearlman, A.L., 1980. Retinotopic organization of striate and extrastriate visual cortex in the mouse. Journal of Comparative Neurology 193, 187–202. doi:10.1002/cne.901930113

Wang, Q., Burkhalter, A., 2013. Stream-Related Preferences of Inputs to the Superior Colliculus from Areas of Dorsal and Ventral Streams of Mouse Visual Cortex. Journal of Neuroscience 33, 1696–1705. doi:10.1523/JNEUROSCI.3067-12.2013

Wang, Q., Burkhalter, A., 2007. Area map of mouse visual cortex. J. Comp. Neurol. 502, 339–357. doi:10.1002/cne.21286

Wang, Q., Gao, E., Burkhalter, A., 2011. Gateways of Ventral and Dorsal Streams in Mouse Visual Cortex. Journal of Neuroscience 31, 1905–1918. doi:10.1523/JNEUROSCI.3488-10.2011

Wang, Q., Sporns, O., Burkhalter, A., 2012. Network Analysis of Corticocortical Connections Reveals Ventral and Dorsal Processing Streams in Mouse Visual Cortex. Journal of Neuroscience 32, 4386–4399. doi:10.1523/JNEUROSCI.6063-11.2012

Wickersham, I.R., Lyon, D.C., Barnard, R.J.O., Mori, T., Finke, S., Conzelmann, K.-K., Young, J.A.T., Callaway, E.M., 2007. Monosynaptic Restriction of Transsynaptic Tracing from Single, Genetically Targeted Neurons. Neuron 53, 639–647. doi:10.1016/j.neuron.2007.01.033

Chapter 2. Functional Differences Between Three Genetically-Defined Layer 5 Cell Types

Abstract

Layer 5 (L5) of visual cortex contains pyramidal cells that can be classified by their anatomy, physiology, and projections. While cortico-cortical (CC) cells project to other cortical regions and striatum, cortico-subcortical (CS) cells project to regions such as the superior colliculus and thalamus. In an effort to relate structure, genetics, connectivity, and function, we characterized the connectivity and intrinsic physiology of genetically-identified L5 cell types that are CC (Tlx-Cre+) or CS (Glt25d2-Cre+). Additionally, we described a third, novel cell type that projects to cortex, but not striatum (CC-NS; Efr3a-Cre+). Here we investigate the function of these three different cell types in vivo using GCaMP6 two-photon imaging. In short, CS cells are more direction selective than CC or CC-NS cells, and all of these L5 cell types are extremely orientation selective. Further, CS cells prefer stimuli at higher temporal frequencies, in line with their role in initiating action via the superior colliculus. Compiled with a comprehensive anatomical and in vitro characterization of these cells, these in vivo imaging findings are a major component of Kim et al., 2015.

Introduction

The mammalian visual cortex is composed of various excitatory and inhibitory cell types arranged in six different layers. Each cortical layer has distinct dynamics, contributing to the integration and distribution of visual information to other cortical as well as subcortical areas (e.g., Briggs and Callaway, 2001; Maier et al., 2010; Olivas

et al., 2012; Ringach et al., 2002; Xing et al., 2012; see Callaway, 1998 for a review). Untangling the computations in canonical microcircuits within and across cortical layers is a critical piece in understanding how the cortex translates sensation into action (Bastos et al., 2012; Harris and Mrsic-Flogel, 2014). Most importantly, understanding these circuits requires matching the genetic and connectivity profile of a cell to its function.

In the past decade, our understanding of different cell types within cortical microcircuits has been significantly aided by numerous mouse lines generated by bacterial artificial chromosome (BAC) constructs, which effectively restrict the expression of Cre recombinase, and ultimately any other protein of interest, to specific cells (Gerfen et al., 2013; Shiaoching Gong et al., 2007; Yang et al., 1997). While most of these Cre-expressing transgenic mouse lines are specific for inhibitory cells with specific calcium binding proteins (Markram et al., 2004; Taniguchi et al., 2011), others mark a certain layer of cortex (Gong et al., 2007; Harris et al., 2014). Such Cre lines have proved incredibly valuable in teasing apart the roles of various cell types in computations such as gain control (Fu et al., 2014; Olsen et al., 2012), surround suppression (Adesnik et al., 2013; Nienborg et al., 2013), and top-down modulation (Zhang et al., 2014)

While there are Cre lines that selectively mark cells of layer 5 (L5; e.g., Rbp4; Gong et al., 2007) this layer of cortex contains various excitatory and inhibitory cell types that likely serve diverse roles in visual processing. L5 excitatory cells, known for their pyramidal shape, are the primary source of V1 output to various cortical and subcortical structures. A large body of research in primates, carnivores, and rats traditionally divides these L5 pyramids into two subclasses based on their anatomy

and projection targets (Bourassa and Deschênes, 1995; Hallman et al., 1988; Hübener and Bolz, 1988; Kasper et al., 1994; Tsiola et al., 2003). Cortico-cortical (CC) cells are located in L5A, remain in the telencephalon (intratelencephalic), are thin-tufted, and project to other cortical regions and the striatum (Groh et al., 2010). On the other hand, cortico-subcortical cells (CS) are found primarily in L5B, are thick-tufted, and project through the pyramidal tract to the superior colliculus, thalamus, and brainstem (Groh et al., 2010).

Despite these observations about the anatomy and connectivity of these L5 cell types, our understanding of their role in visual processing is largely incomplete. Until recently, identifying a cell by its projections has been limited to using antidromic stimulation. Such studies in cats have demonstrated that CS cells are very direction-selective, presumably to guide eye movements (Palmer and Rosenquist, 1974). On the other hand, CC cells are thought to be involved in image formation, but this has not been directly studied (Van Essen, 2005).

Studying the role of these L5 cell types in visual processing would be greatly aided by Cre lines and corresponding genetic tools to target them. Recently, our lab has identified three GENSAT mouse lines that mark layer 5 cells with restricted projection patterns (Gerfen et al., 2013; Kim et al., 2015). These genetically-identified cell types faithfully mark CC (Tlx3-Cre) and CS (Glt25d2-Cre) cell types, with morphology and intrinsic physiology that is consistent with their descriptions in other mammalian species (Kim et al., 2015). In addition, we identified a third type of L5 cell in mouse that is similar to CC cells, but does not project to the striatum and is therefore termed cortico-cortical non-striatal (CC-NS; Cowan and Wilson, 1994; Lévesque et al., 1996).

Because L5 CC, CC-NS, and CS pyramidal neurons have distinct anatomical and electrophysiological profiles and project to different structures, it is likely that they have different computational abilities and process different types of visual information. We therefore took advantage of the Tlx3-Cre, Glt25d2-Cre, and Efr3a-Cre mouse lines to investigate the in vivo functional properties of L5 CC, CC-NS, and CS PNs in mouse V1. Using these transgenic mice in combination with Cre-dependent expression of the genetically-encoded calcium indicator GCaMP6, we can bridge connectivity and behavior in visual cortex.

Results

Visual response properties were characterized based on two-photon imaging of calcium dynamics in stationary, awake mice (Figure 2.1). We expressed the calcium indicator GCaMP6 and tdTomato in subsets of CC, CC-NS, or CS L5 PNs by injecting a 2:1 mixture of AAV-FLEX-GCaMP6 and AAV-FLEX-tdTomato in V1 of each Cre transgenic mouse (Figure 2.1). Figure 2.1B displays a z stack of two-photon microscope images from GCaMP6 and tdTomato expressing L5 CS PNs in V1 of a Glt25d2-Cre mouse; cell bodies can be clearly distinguished as well as their apical dendrites extending through the cortical depth up to the pia.

To assess tuning properties, two different stimulation paradigms were used. To quantify spatial frequency (SF) tuning, drifting sine wave gratings were varied over five different SFs (0.01 to 0.16 cycles per degree, c/d) and eight different directions while temporal frequency (TF) was kept constant at 1 Hz. To quantify TF tuning, gratings were presented at five different TFs (0.5 to 8 Hz) and eight directions, while SF was kept constant at 0.04 c/d. Using these paradigms, we recorded calcium

transients and generated tuning curves for SF, TF, and orientation/direction (at best SF or TF) for Tlx3-Cre+, Glt25d2-Cre+, and L5 Efr3a-Cre+ neurons (Figures 2.2 & 2.3).

For neurons that were visually responsive and reliable (see Experimental Procedures), various indices were calculated: orientation selectivity (OSI), direction selectivity (DSI), preferred SF, and preferred TF (Figure 2.3). We present data for both SF and TF paradigms for Tlx3-Cre+and Glt25d2-Cre+ neurons, but only for the SF paradigm for L5 Efr3a-Cre+ neurons because L5 Efr3a-Cre+ neurons tended to prefer very high SF and were therefore rarely responsive to the lower SF gratings used in the TF paradigm (see details below).

To compare visual response properties between the L5 cell types in V1, we characterized the visual responses (OSI, DSI, TF, and SF) of more than 110 Tlx3-Cre+, 13 Glt25d2-Cre+, and 17 L5 Efr3a-Cre+ neurons (Figure 2.3). Comparisons of the distributions of preferred SF between the three cell types (Figure 2.3) showed that both L5 Efr3a-Cre+ and Glt25d2-Cre+ cells tended to prefer higher SF than Tlx3-Cre+ cells (median 0.04 c/d for Tlx3-Cre+ and 0.08 c/d for both Glt25d2-Cre+ and L5 Efr3a-Cre+), but only the distribution for L5 Efr3a-Cre+ cells differed significantly from Tlx3-Cre+ cells (Kruskal-Wallis test, $p = 0.0015$, with Dunn's multiple comparisons L5 Efr3a-Cre+ versus Tlx3-Cre+, $p = 0.0019$). The distributions for Tlx3-Cre+ and Glt25d2-Cre+ cells are similar to previous reports for mouse V1 L2/3 neurons (Marshel et al., 2011; Niell and Stryker, 2008a). However, L5 Efr3a-Cre+ neurons appear unique in their SF preference: the majority of cells (14/17, 82%) prefer a SF of 0.08 or higher. While Glt25d2-Cre+ and Tlx3-Cre+ neurons did not differ significantly in their SF tuning, these populations did differ significantly in TF tuning (Figure 2.3),

with Glt25d2-Cre+ neurons preferring TFs that were nearly twice as fast as for Tlx3-Cre+ neurons (median 4.0 Hz and 2.0 Hz respectively, Wilcoxon rank-sum test, and $p = 0.0242$). All three cell types were highly orientation tuned. Across SF and TF experiments, Glt25d2-Cre+ were the least tuned, yet still had median OSI values > 0.61, and over two-thirds of cells had an OSI > 0.5 (see Figure 2.3 for values for all cell types.)

Using the varied SF paradigm with TF held constant at 1 Hz, L5 CS PNs were remarkably direction selective and non-parametric statistical tests showed that Glt25d2-Cre+ neurons have higher DSI (median 0.57) than Tlx3-Cre+ (median 0.24, Kruskal- Wallis test, $p = 0.0024$, with Dunn's multiple comparisons, Tlx3-Cre+ versus Glt25d2-Cre+, $p = 0.0135$). There were 60% of Glt25d2-Cre+ cells that were very sharply tuned for direction (DSI > 0.5), while less than 30% of Tlx3-Cre+ or L5 Efr3a-Cre+ cells had DSI > 0.5 (Figure 2.3, top right). Interestingly, when TF was varied and SF was held constant at 0.04 c/d, the DSI values for Glt25d2-Cre+ neurons were lower than in the SF paradigm (median 0.46), while the DSI values were similar for Tlx3- Cre+ neurons regardless of the stimulation paradigm (median 0.34) and differences between the distributions were not statistically significant. In summary, L5 Efr3a-Cre+ neurons prefer higher SFs than Tlx3-Cre+, Glt25d2-Cre+ neurons prefer higher TFs than Tlx3-Cre+, and Glt25d2-Cre+ are more direction selective than Tlx3-Cre+ cells.

Discussion

While previous in vitro studies have provided extensive information about the intrinsic physiology and local connectivity of specific cortical cell types, an

understanding of in vivo function has been more elusive. Our observations reveal novel insights into the diversity of L5 pyramidal cells, demonstrating functional differences that may underlie their unique contributions to perception or action.

Using two-photon calcium imaging, we have shown that L5 neurons exhibit diverse *in vivo* responses. Glt25d2-Cre+ V1 neurons have greater selectivity for direction and prefer higher TFs compared to Tlx3-Cre+ V1 neurons. This indicates that Glt25d2-Cre+ neurons and Tlx3-Cre+ neurons integrate and convey different visual information to downstream target regions. Furthermore, Efr3a-Cre+ neurons prefer higher SFs than both Tlx3-Cre+ neurons, suggesting that these cells are involved in pathways requiring higher visual acuity. Lastly, we found that each of these cell types were highly orientation tuned, more so than those reported in previous studies using single-unit electrical recordings in L5 of anesthetized or awake mice (Niell and Stryker, 2010; 2008b). It should be noted that only about 10%–20% of L5 neurons responded reliably to the drifting grating stimuli we used (Table 2.1). This is lower than the roughly 50% of visually responsive neurons in L2/3, but comparable to the low percentages in some extrastriate visual areas (Andermann et al., 2011; Marshel et al., 2011). Future studies should investigate experimental conditions and/or stimuli that might generate responses in neurons that were not responsive under our experimental conditions.

Previous studies of functional properties and connections in primate, cat, and rodent V1 also suggest that CC PNs process and convey image-forming visual information to higher visual cortices, whereas CS PNs are involved in sensory gating associated with movement (Finlay et al., 1976; Palmer and Rosenquist, 1974; Van Essen, 2005). Consistent with their projections to higher-order visual cortices and

preferences for higher spatial frequencies, L5 CC cells may convey feedforward visual information necessary for object/place recognition or multimodal integration. In contrast, L5 CS cells are quite selective for direction and send visual motion-related information to the superior colliculus.

Our work here provides a basis to probe these cells types even further with cell-specific optogenetic manipulation. Future studies in the lab will investigate the role of these cells in visual cortex computations (e.g. layer specific gain control) and visually-guided behaviors (e.g. attention), as well as their single-cell input-output connectivity to other cortical regions.

Experimental Procedures

Transgenic mice. All experimental procedures followed procedures approved by the Salk Institute Animal Care and Use Committee. Tlx3-Cre PL56, Glt25d2-Cre (or Colgalt2-Cre) NF107 and Efr3a-Cre NO108 mice are GENSAT BAC transgenic lines and have been previously described (Gerfen et al., 2013; Gong et al., 2007). Mouse strains were maintained on mixed genetic backgrounds (129/C57BL6).

AAV Injections. A 2:1 mixture of AAV1.CAG.Flex.GCaMP6f.WPRE.SV40 (3.06X1013 GC/ml) or AAV1.hSyn.Flex.GCaMP6s.WPRE.SV40 (3.63X1013 GC/ml) from Penn Vector Core and AAV-FLEX-tdTomato.Virus was injected into the center of V1, using the following coordinates: 3.4 mm rostral, 2.6 mm lateral relative to bregma and 0.5-0.7 mm ventral from the pia. We injected 100nl of AAVs using either air pressure by picospritzer (General Valve Corp, Fairfield, NJ) or performed iontophoresis (Precision Current Source, Stoelting Co., Wood Dale, IL) at +3- 5 μA set to alternate on for 7 second and off for 7 second for 5 minutes.

Mouse preparation. Experiments were performed on 2-4 month old transgenic mice (male and female) approximately 7-15 days after GCaMP6 virus injection. Animals were anesthetized with inhaled isoflurane (0.5-1.2% in oxygen) and carprofen (5 mg/kg SC) and custom circular head frames were mounted to the skull with dental acrylic (C&B-Metabond®). Eyes were kept moist with ointment during surgeries. A 5-6mm diameter craniotomy was made over V1 and the dura was also removed. Dura removal proved necessary for clear imaging in layer 5 (475-620 μm deep, Figure 2.1). The brain was covered with a cranial window, consisting of a 4 or 5 mm coverslip and a metal ring designed to fit within the headframe. Pressure was gently applied to the brain upon placement of the window. After implantation of the window, the mouse was allowed to wake up, and imaging began when the mouse was fully awake. For several mice, imaging was performed over multiple days. These mice were housed with ibuprofen medicated water. During imaging, mice were stationary and positioned in a plastic cylinder to restrict movement. Imaging was done with a custom-made scope (Marshel et al., 2011) and ScanImage 3.8 with scan parameters 256x256 lines/frame at 2 msec/line. GCaMP6 was excited at 920 or 940 nm at high power of Ti:Sapphire laser (Coherent), and emission was collected with a green (535 ± 50 nm or 525 ± 50 nm) and a red (610 ± 75 nm or 610 ± 60 nm) filter (Chroma).

Visual stimuli for two-photon imaging. Mice were positioned 13 cm from a video monitor, which was centered on their eye and pointed towards their nose at a 30° angle. Stimuli were 4 sec duration, 100% contrast sine wave grating moving in 8 different directions. For each population of neurons (a single 16x imaging plane, with 1-2.5x digital zoom), we presented two sets of stimuli: a temporal frequency (TF)

varying experiment (0.5, 1, 2, 4, and 8 Hz, 8 directions plus blank, 0.04 c/d, 5 repeats pseudorandomized), and a spatial frequency (SF) varying experiment (0.01, 0.02, 0.04, 0.08, and 0.16 c/d, 8 directions plus blank, 1 Hz, 5 repeats pseudorandomized) The stimulus was spherically corrected to account for distortions in size and spatial frequency at the periphery, effectively keeping SF and TF constant throughout the visual field (Marshel et al., 2011). Stimuli were generated by a customized PsychToolbox interface in MATLAB (I. Nauhaus).

Analysis of calcium imaging data. Regions of interest (ROIs) around each cell were created using a semi-automatic cell segmentation method (Marshel et al., 2011). To account for movement-related image shifts as well as drifts in the image over time, we used a procedure involving multiple movement correction algorithms both in ImageJ (using StackReg and Template Matching plugin) and a customized movement correction algorithm in MATLAB (Marshel et al., 2011) that aligned each trial of the experiment to the average image of the first trial by determining the highest cross-correlation between images. The type of motion correction algorithm used depended on the severity of motion. Each experiment was manually checked to ensure motion had been effectively corrected. Any field of view with uncorrectable x-y shifts or evidence of z-motion was discarded. Baseline fluorescence (FB) was averaged within each cell ROI for each trial during a 2 sec prestimulus period during which a gray screen (mean luminance of gratings) was presented. The stimulus-evoked time course was converted from absolute to relative fluorescence by computing $\Delta F/F = (FI-FB)/FB$, where FI is the average instantaneous, stimulus-evoked fluorescence signal over the duration of the stimulus (4 sec).

Identification of responsive and reliable cells. The population analysis was restricted to cells that were both responsive (ΔF/F > 6%) and reliable as determined by a D-prime metric, defined as $\delta=(\mu_{max}-\mu_{blank})/(\sigma_{max}+\sigma_{blank})$ where μ_{max} and σ_{max} are the mean and standard deviation of the response to the preferred stimulus, and μ_{blank} and σ_{blank} are the mean and standard deviation to the blank stimulus. Neurons were deemed reliable for $\delta>1$. The neurons that met these criteria were used as the denominator in all subsequent analyses. Any field of view that did not have at least one cell meeting the criteria was discarded. Due to a slow decay in the fluorescence over the 4 second imaging period, even during the blank screen, we baseline corrected the ΔF/F by subtracting the mean ΔF/F during the blank stimulus. This assures that stimulus-evoked values are in relation to a proper baseline corrected for bleaching of the fluorescence, likely due to the higher laser power necessary for deep imaging. These corrected ΔF/F values were used to construct tuning curves and derive cell metrics, but did not contribute to the identification of responsive and reliable cells. The indices (OSI and DSI) were defined as $SI = (\mu_{max} - \mu_{null}) / (\mu_{max} + \mu_{null})$ where μ_{max} is the mean response to the preferred direction and μ_{null} is the mean response to the opposite direction for DSI, and the average of the two orthogonal directions for OSI. As some cells suppressed their response below the blank baseline response for null orientations, the OS and DS indices were occasionally above 1.0.

Figures and Tables

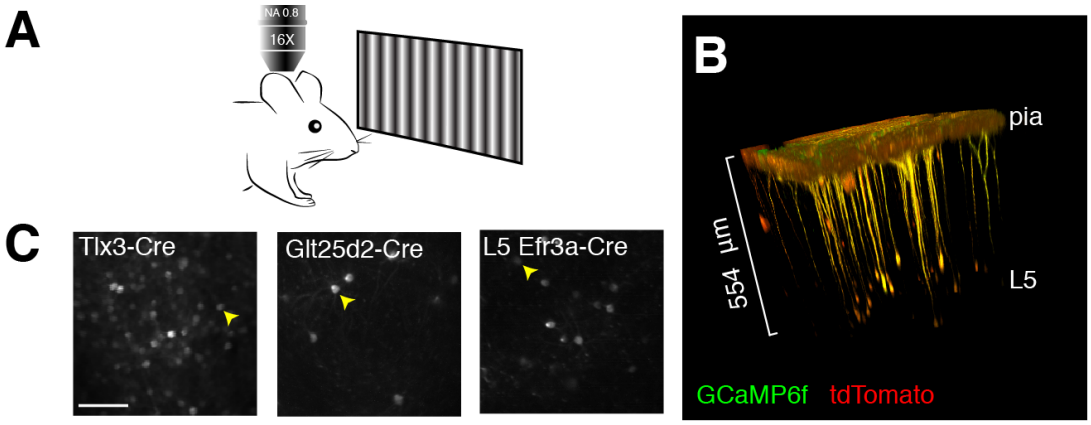

Figure 2.1. Two-photon imaging of layer 5 in vivo. (A) Schematic illustration of two-photon in vivo calcium imaging set up for awake and head-fixed stationary mouse. (B) Two-photon microscope z stack projection of Glt25d2-Cre+ mouse V1 after AAV-FLEX-GCaMP6 and AAV-FLEX-tdTomato injection. (C) Representative images of single cells expressing GCaMP6 in V1 of Tlx3-Cre+, Glt25d2-Cre+, and Efr3a- Cre+ mice. The arrowheads indicate cells plotted in Figure 2.3. The scale bar represents 100 mm.

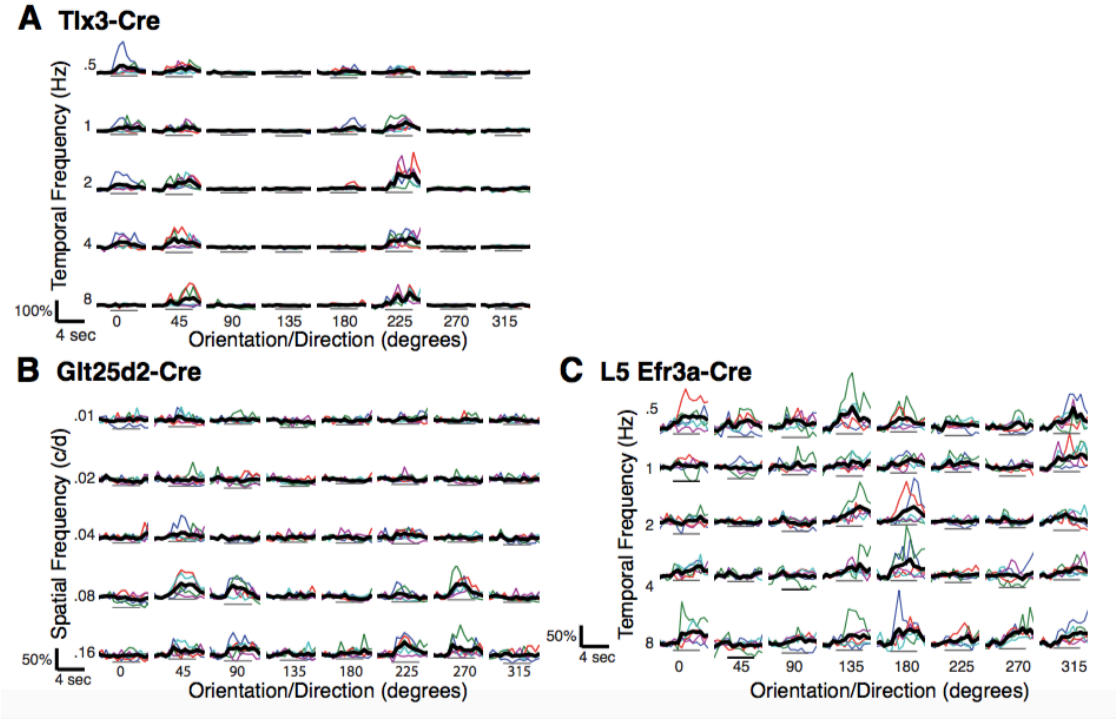

Figure 2.2. Sample traces from two-photon GCaMP6 recordings of L5 pyramidal cells. (A-C) Fluorescence changes in response to drifting gratings in 8 different directions. Each panel shows all of the responses (5 repeats) for a single neuron to a specific direction and spatial or temporal frequency. Gray lines under each trace indicate duration of stimulus. Thick black traces indicate averaged responses across five repeats. (A) Fluorescence traces for a V1 Tlx3-Cre+ cell at five different temporal frequencies (TFs). (B) Fluorescence traces for Glt25d2-Cre+ cell at 5 different spatial frequencies (SFs). (C) Fluorescence traces for L5 Efr3a-Cre+ cell at 5 different TFs.

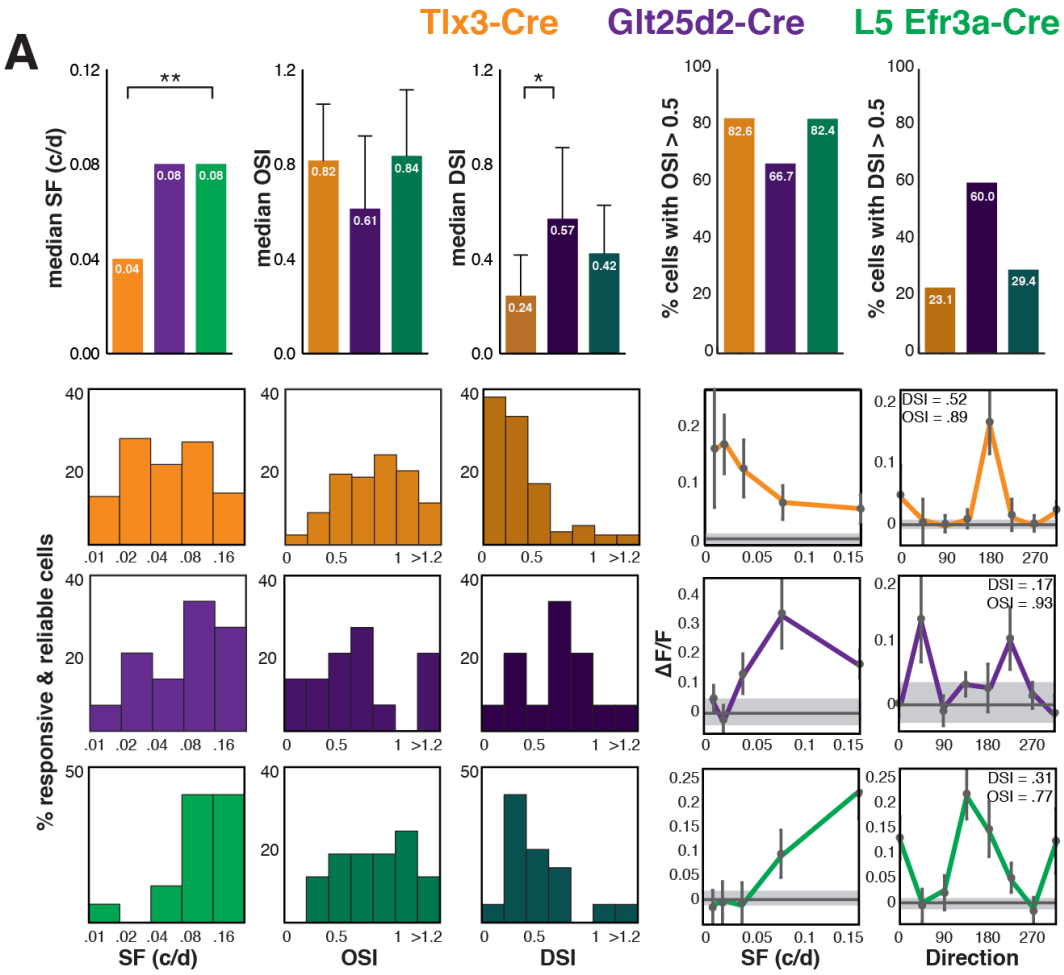

Figure 2.3 Population summary of visual responses in three different types of L5 pyramidal neurons. (A) SF experiments. The top image shows medians for preferred SF, OSI, and DSI (with interquartile ranges for OSI and DSI, at the preferred SF) for Tlx3-Cre+, Glt25d2-Cre+, and L5 Efr3a-Cre+ neurons, as well as the percentage of cells with OSI or DSI > 0.5. The bottom left image shows distributions of preferred SF, OSI, and DSI (at the preferred SF) for Tlx3-Cre+, Glt25d2-Cre+, and L5 Efr3a-Cre+ neurons. The bottom right image shows SF and orientation tuning curve examples for each cell type. The values are plotted as means ± SEM. The gray lines indicate average responses during blank stimulus; the shading is ±SEM. (B) TF experiments. The top image shows medians with interquartile ranges for preferred TF, OSI, and DSI (at the preferred TF) for Tlx3-Cre+ and Glt25d2-Cre+ neurons, as well as the percentage of cells with OSI or DSI > 0.5. The bottom left image shows distributions of preferred TF, OSI, and DSI (at the preferred TF) for Tlx3-Cre+ and Glt25d2Cre+ neurons. The bottom right image shows TF and orientation tuning curve examples for each cell type. The values are plotted as means ± SEM. The gray lines indicate average responses during blank stimulus; the shading is ±SEM. For the median plots, the statistical significances are labeled as p values after Wilcoxon rank-sum test (TF experiments) or Kruskal-Wallis test with Dunn's multiple comparisons test as post hoc (SF experiments) (*p < 0.05 and **p < 0.01). Abbreviations: c/d, cycle per degree; Hz, Hertz.

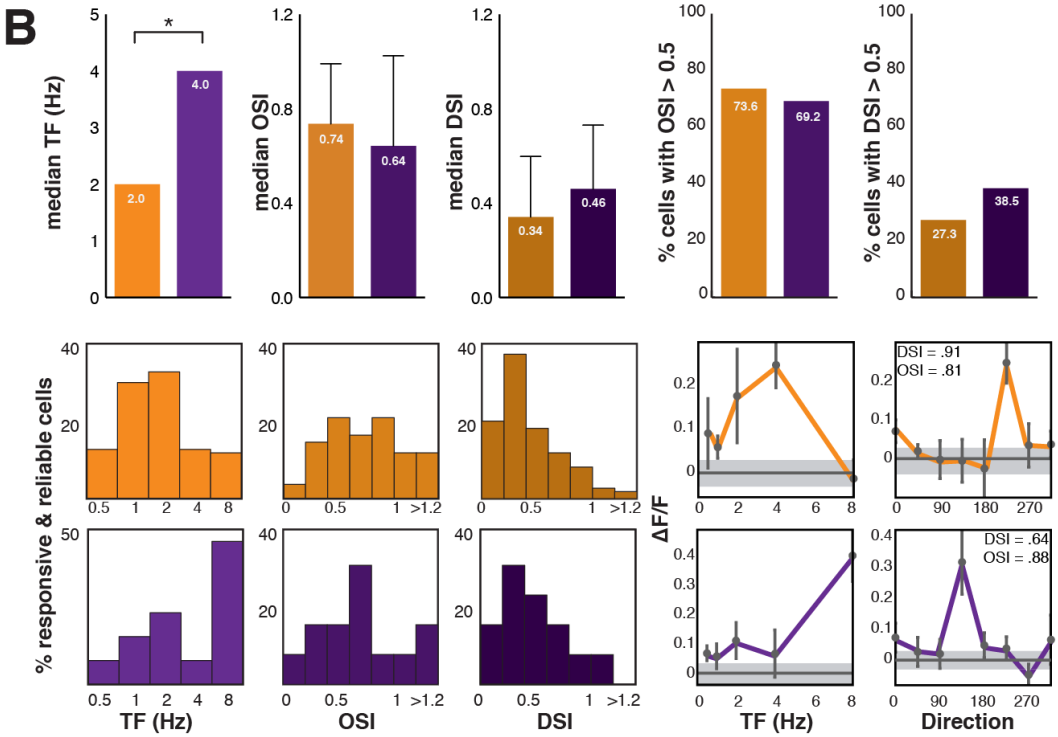

Figure 2.3 Population summary of visual responses in three different types of L5 pyramidal neurons (continued).

Table 2.1. Summary of in vivo two-photon calcium imaging experiments. Total cells are total counted cells in all fields of view. Responsive cells are cells with response magnitudes greater than 6% ΔF/F. Reliable cells are cells with D-prime metric > 1. Responsive & reliable meet both of these criteria.

	Mice	Fields of View	Total Cells	Responsive Cells	Reliable Cells	Responsive & Reliable Cells
SF Experiments						
Tlx3-Cre	5	10	1805	582(32.2%)	211(11.7%)	121(6.7%)
Glt25d2-Cre	8	12	196	61(31.1%)	25(12.8%)	15(7.65%)
Efr3a-Cre	3	4	79	36(45.6%)	23(29.1%)	17(21.5%)
TF Experiments						
Tlx3-Cre	3	10	2328	788(33.8%)	251(10.8%)	110(4.73%)
Glt25d2-Cre	6	8	163	44(27.0%)	24(14.7%)	13(7.98%)

Acknowledgements

This work was completed in collaboration with Euiseok Kim, Espoir Kyubwa, Matthew Jacobs, and Edward Callaway. I would like to thank this talented team for their diversity of skills and input. This work exemplifies the unique range of techniques and knowledge possessed by our lab.

In addition, we would like to thank B.J. Neichin, T. Ito, D. Chatterjee, and S. Gilmour for technical assistance; I. Nauhaus for programming help; C. Gerfen and E. Schmidt for BAC transgenic mice search help. We also thank the Salk Viral Vector and Biophotonics Core staff members. This work was supported by the NIH grants EY022577, EY019005, and MH063912 and the Gatsby Charitable Foundation (E.M.C.). A.L.J. is supported by the National Science Foundation and Martinet Foundation. E.M.K. is supported by the Howard Hughes Medical Institute Gilliam Fellowship and the University of California, San Diego Medical Scientist Training Program T32 GM007198-40. E.J.K. is a Biogen-IDEC Fellow of the Life Science Research Foundation and a recipient of the 2012 NARSAD Young Investigator Award from the Brain & Behavior Research Foundation.

Chapter 2, in part, is a reprint of the material as it appears in Kim. E.J., Juavinett, A.L., Kyubwa, E.M., Jacobs, M.W., Callaway, E.M. (2015). Three Types of Cortical Layer 5 Neurons That Differ in Brain-wide Connectivity and Function. *Neuron* 88(6): 1253-67. The dissertation author was the second author in this collaborative effort.

References

Adesnik, H., Bruns, W., Taniguchi, H., Huang, Z.J., Scanziani, M., 2013. A neural circuit for spatial summation in visual cortex. Nature 490, 226–231.

Bastos, A.M., Usrey, W.M., Adams, R.A., Mangun, G.R., Fries, P., Friston, K.J., 2012. Canonical microcircuits for predictive coding. Neuron 76, 695–711.

Bourassa, J., Deschênes, M., 1995. Corticothalamic projections from the primary visual cortex in rats: a single fiber study using biocytin as an anterograde tracer. Neuroscience 66, 253–263. doi:10.1016/0306-4522(95)00009-8

Briggs, F., Callaway, E.M., 2001. Layer-specific input to distinct cell types in layer 6 of monkey primary visual cortex. J. Neurosci. 21, 3600–3608.

Callaway, E.M., 1998. LOCAL CIRCUITS IN PRIMARY VISUAL CORTEX OF THE MACAQUE MONKEY. Annu. Rev. Neurosci 21, 47–74.

Cowan, R.L., Wilson, C.J., 1994. Spontaneous firing patterns and axonal projections of single corticostriatal neurons in the rat medial agranular cortex. J. Neurophysiol. 71, 17–32.

Finlay, B.L., Schiller, P.H., Volman, S.F., 1976. Quantitative studies of single-cell properties in monkey striate cortex. IV. Corticotectal cells. J Neurophysiol.

Fu, Y., Sheng, N., Darcy, D.P., Tucciarone, J.M., Espinosa, J.S., Nicoll, R.A., Huang, Z.J., Sheng, N., Stryker, M.P., Darcy, D.P., Nicoll, R.A., Huang, Z.J., Stryker, M.P., 2014. A Cortical Circuit for Gain Control by Behavioral State. Cell 156, 1139–1152.

Gerfen, C.R., Paletzki, R., Heintz, N., 2013. GENSAT BAC Cre-Recombinase Driver Lines to Study the Functional Organization of Cerebral Cortical and Basal Ganglia Circuits. Neuron 80, 1368–1383. doi:10.1016/j.neuron.2013.10.016

Gong, S., Doughty, M., Harbaugh, C.R., Cummins, A., Hatten, M.E., Heintz, N., Gerfen, C.R., 2007. Targeting Cre Recombinase to Specific Neuron Populations with Bacterial Artificial Chromosome Constructs. J. Neurosci. 27, 9817–9823. doi:10.1523/JNEUROSCI.2707-07.2007

Gong, S., Doughty, M., Harbaugh, C.R., Cummins, A., Hatten, M.E., Heintz, N., Gerfen, C.R., 2007. Targeting Cre Recombinase to Specific Neuron Populations with Bacterial Artificial Chromosome Constructs. J. Neurosci. 27, 9817–9823. doi:10.1523/JNEUROSCI.2707-07.2007

Groh, A., Meyer, H.S., Schmidt, E.F., Heintz, N., Sakmann, B., Krieger, P., 2010. Cell-type specific properties of pyramidal neurons in neocortex underlying a layout that is modifiable depending on the cortical area. Cereb. Cortex 20, 826–836. doi:10.1093/cercor/bhp152

Hallman, L.E., Schofield, B.R., Lin, C.S., 1988. Dendritic morphology and axon collaterals of corticotectal, corticopontine, and callosal neurons in layer V of primary visual cortex of the hooded rat. J. Comp. Neurol. 272, 149–160. doi:10.1002/cne.902720111

Harris, J. a., Hirokawa, K.E., Sorensen, S. a., Gu, H., Mills, M., Ng, L.L., Bohn, P., Mortrud, M., Ouellette, B., Kidney, J., Smith, K. a., Dang, C., Sunkin, S., Bernard, A., Oh, S.W., Madisen, L., Zeng, H., 2014. Anatomical characterization of Cre driver mice for neural circuit mapping and manipulation. Front. Neural Circuits 8, 1–16. doi:10.3389/fncir.2014.00076

Harris, K.D., Mrsic-Flogel, T.D., 2014. Cortical connectivity and sensory coding. Nature 503, 51–58.

Hübener, M., Bolz, J., 1988. Morphology of identified projection neurons in layer 5 of rat visual cortex. Neurosci. Lett. 94, 76–81. doi:10.1016/0304-3940(88)90273-X

Kasper, E.M., Larkman, A.U., Lubke, J., Blakemore, C., 1994. Pyramidal neurons in layer 5 of the rat visual cortex. I. Correlation among cell morphology, intrinsic electrophysiological properties, and axon targets. J. Comp. Neurol. 339, 459–474. doi:10.1002/cne.903390402

Kim, E.J., Juavinett, A.L., Kyubwa, E.M., Jacobs, M.W., Callaway, E.M., 2015. Three Types of Cortical Layer 5 Neurons That Differ in Brain-wide Connectivity and Function. Neuron 88, 1–16.

Lévesque, M., Charara, A., Gagnon, S., Parent, A., Deschenes, M., 1996. Corticostriatal projections from layer V cells in rat are collaterals of long -range corticofugal axons. Brain Res. 709, 311–315.

Maier, A., Adams, G.K., Aura, C., Leopold, D. a, 2010. Distinct superficial and deep laminar domains of activity in the visual cortex during rest and stimulation. Front. Syst. Neurosci. 4, 1–11. doi:10.3389/fnsys.2010.00031

Markram, H., Toledo-Rodriguez, M., Wang, Y., Gupta, A., Silberberg, G., Wu, C., 2004. Interneurons of the neocortical inhibitory system. Nat. Rev. Neurosci. 5, 793–807.

Marshel, J.H., Garrett, M.E., Nauhaus, I., Callaway, E.M., 2011. Functional Specialization of Seven Mouse Visual Cortical Areas. Neuron 72, 1040–1054.

Nienborg, H., Hasenstaub, A., Nauhaus, I., Taniguchi, H., Huang, Z.J., Callaway, E.M., 2013. Contrast dependence and differential contributions from somatostatin- and parvalbumin-expressing neurons to spatial integration in mouse V1. J. Neurosci. 33, 11145–11154.

Olivas, N.D., Quintanar-Zilinskas, V., Nenadic, Z., Xu, X., 2012. Laminar circuit organization and response modulation in mouse visual cortex. Front. Neural Circuits 6, 1–21. doi:10.3389/fncir.2012.00070

Olsen, S.R., Bortone, D.S., Adesnik, H., Scanziani, M., 2012. Gain control by layer six in cortical circuits of vision. Nature 483, 47–52.

Palmer, L.A., Rosenquist, A.C., 1974. Visual receptive fields of single striate cortical units projecting to the superior colliculus in the cat. Brain Res. 67, 27–42. doi:10.1016/0006-8993(74)90295-9

Ringach, D.L., Shapley, R.M., Hawken, M.J., 2002. Orientation selectivity in macaque V1: diversity and laminar dependence. J. Neurosci. 22, 5639–5651. doi:20026567

Taniguchi, H., He, M., Wu, P., Kim, S., Paik, R., Sugino, K., Kvitsiani, D., Kvitsani, D., Fu, Y., Lu, J., Lin, Y., Miyoshi, G., Shima, Y., Fishell, G., Nelson, S.B., Huang, Z.J., 2011. A resource of Cre driver lines for genetic targeting of GABAergic neurons in cerebral cortex. Neuron 71, 995–1013. doi:10.1016/j.neuron.2011.07.026

Tsiola, A., Hamzei-Sichani, F., Peterlin, Z., Yuste, R., 2003. Quantitative morphologic classification of layer 5 neurons from mouse primary visual cortex. J. Comp. Neurol. 461, 415–428. doi:10.1002/cne.10628

Van Essen, D.C., 2005. Corticocortical and thalamocortical information flow in the primate visual system. Prog. Brain Res. 149, 173–185. doi:10.1016/S0079-6123(05)49013-5

Xing, D., Yeh, C.I., Burns, S., Shapley, R.M., 2012. Laminar analysis of visually evoked activity in the primary visual cortex. Proc Natl Acad Sci U S A 109, 13871–13876. doi:10.1073/pnas.1201478109

Yang, X.W., Model, P., Heintz, N., 1997. Homologous recombination based modification in Escherichia coli and germline transmission in transgenic mice of a bacterial artificial chromosome. Nat. Biotechnol. 15, 859–65. doi:10.1038/nbt0997-859

Zhang, S., Xu, M., Kamigaki, T., Do, J.P.H., Chang, W.-C., Jenvay, S., Miyamichi, K., Luo, L., Dan, Y., 2014. Long-range and local circuits for top-down modulation of visual cortex processing. Science (80-.). 345, 660–665.

Chapter 3. Topographical organization of the mouse lateral posterior thalamic nucleus

Abstract

The visual thalamus is critical hub for incoming sensory information, though the role of the abundant feedforward and feedback connectivity between the thalamus and cortex remains elusive. Primate pulvinar is topographically and functionally organized, but a more granular connectivity map is needed to understand the role of thalamocortical loops in visually guided behavior. Similarly, the secondary visual thalamic nucleus in mice (the lateral posterior nucleus, LP) has extensive connections with cortex. To resolve the precise connectivity of these circuits, we first mapped mouse visual cortex using intrinsic signal optical imaging and then injected fluorescently tagged retrograde tracers (cholera toxin subunit B) into various combinations of six different visual areas. We find that LP has separate zones that project to specific extrastriate regions, with few cells (~4-6%) projecting to multiple visual areas. Additional experiments will investigate cortical and subcortical input to LP cells with known extrastriate projection targets using a rabies tracing approach. Disentangling these circuits will yield important insights into the role of the secondary visual thalamus in sensory processing and guide future functional studies.

Introduction

While the classic description of the visual system depicts information in parallel streams traveling up a hierarchy, this illustration is complicated by the fact that there is a tremendous amount of feedback to the lateral geniculate nucleus

(LGN), as well as to the secondary visual thalamic nucleus, the pulvinar (Felleman and Van Essen 1991). A relatively large structure that is extensively connected with various areas of cortex, the pulvinar is thought to be involved in a variety of complex behaviors. In primates and carnivores, pulvinar is implicated in attention (e.g., Chalupa et al., 1976; Desimone et al., 1990) as well as multimodal processing (e.g. Chalupa and Fish, 1978; Gattass et al., 1978), and has been shown to exhibit pattern direction selective responses to plaids (Merabet et al., 1998; Villeneuve et al., 2005). Still, the contributions of each of these pathways to responses in subcortical and cortical areas and to perception are unknown, and investigating LP/pulvinar function would be greatly aided by a more precise map of its connections. It is necessary to delineate these thalamocortical pathways so that we can investigate the mechanisms of higher-order visual processing with cell-type and region-specific detail.

In cats and rodents, the lateral posterior nucleus of the thalamus (LP) is considered to be the homologue of primate pulvinar based on its reciprocal connectivity with various regions of visual, parietal, and frontal cortex and abundant input from the superior colliculus (SC; Lent, 1982). Unlike LGN which only receives layer 6 input, LP/pulvinar receives input from both layer 5b and 6 (Gilbert and Kelly, 1975; Li et al., 2003b; Roth et al., 2015). A single-cell tracing study in the rat suggests based on anatomical features that layer 5b inputs are driving, type-II synapses, whereas layer 6 inputs are “modulatory,” type-I synapses (Bourassa and Deschênes, 1995; Sherman and Guillery, 1998), and additional studies have shown that these inputs are restricted to specific regions of LP (Li et al., 2003b).

In rats, hamsters, and cats, LP can be divided into several subdivisions (LPLR, LPLC, LPCM, LPRM), based on its cytoarchitecture and connectivity to

cortical and subcortical areas (Abramson and Chalupa, 1988; Conte et al., 2008; Kamishina et al., 2009, 2008; Reep and Corwin, 2009; Sukekawa, 1988; Takahashi, 1985). There are several consistent observations about inputs to LP in mice; for example, ganglion cells in the retina project to LPMR, while medial prefrontal cortex projects to LPLR (Allen et al., 2016; Noseda et al., 2010; Sukekawa, 1988). Furthermore, LP/pulvinar in rodents, cats, and primates is topographically organized, with different subdivisions connecting to specific regions of cortex (Le Gros Clark, 1932; Shipp, 2003; Mason, 1978; Tohmi et al., 2014). To date, no detailed study of this topography has been completed in the mouse.

Beyond some speculation based on its broad connectivity, little is known about the function of LP (Reep and Corwin, 2009; Sukekawa, 1988). Cells in LP are clearly visually responsive and retinotopically organized, and many exhibit clear ON and OFF receptive fields (Allen et al., 2016). Compared to LGN, LP seems to be more involved with signaling visuomotor mismatch, a role that is likely enabled by its broad connectivity with visual and motor cortices, as well as SC (Roth et al., 2015). Indirect evidence also suggests that LP and the extrageniculate pathway may contribute to information processing in visual cortex, as lesioning the SC caused a shift in the speed-tuning of V1 (Tohmi et al., 2014). While this study indirectly implicates LP in contributing to the visual responses of V1 cells, it does not provide direct evidence that LP, not SC, is necessary for these computations.

Although the coarse connectivity between LP/pulvinar and mouse visual cortex has been reported, these descriptions need to be updated in light of our increasing appreciation for the organization of mouse visual cortical areas (Andermann et al., 2011; Garrett et al., 2014; Huberman and Niell, 2011; Marshel et

al., 2011; Niell, 2011). In addition to a full description of its topography, there are several open questions about the projection patterns of individual cells in LP. For instance, does a cell in LP project to one, or multiple visual areas? If so, is there an apparent functional organization of these inputs to cortex, possibly underlying the visual function of those regions? Mapping the connections between LP and cortex will shed light on whether LP serves to pass information up the cortical hierarchy, or rather acts as a loop within various visual areas, perhaps for the purposes of synchronizing information streams. With this approach, we hope to elucidate the role of LP in the mouse, providing a framework against which we can test various theories of thalamocortical circuit function (Crick and Koch, 1998; Grieve et al., 2000; Olshausen et al., 1993), particularly related to drivers and modulators (Sherman and Guillery, 1998) and the role of the thalamus as a gate for sensory information.

Results

We investigated the topographic organization of thalamocortical projections by first mapping visual cortex and then injecting retrograde tracers into six different visual areas. In each mouse, we first mapped the retinotopic organization of the visual cortex using intrinsic signal imaging (Figure 3.1). Using these maps, we automatically constructed borders between visual areas (Garrett et al., 2014) and targeted the injection of an efficient retrogradely transported neuroanatomical tracer, cholera toxin subunit B (CTB), conjugated to various Alexa fluorophores (Figure 3.1; AF-CTB).

With 23 injections of AF-CTB into six different visual areas in 12 mice, we find that well-segregated zones of LP project to different visual areas, and that these

patterns were reproducible across many animals (Figure 3.2). There was a notable segregation between LM and PM projecting neurons, with PM projecting neurons located in very anterior/medial LP, and LM projecting neurons in lateral/posterior LP. RL, AM, and AL all had clear projections from the most dorsal aspect of Po in addition to LP. By aligning each section onto a common atlas section (Paxinos and Franklin, 2013), we were able to compute average projection regions and observe the topographical organization of LP projections to cortex (Figure 3.2).

By injecting 2-3 different AF-CTBs into each mouse, we could identify the percent of overlap between projections to different visual areas (Figure 3.3). Across areas, there were very few cells that projected to more than one visual area (~4-6% of all retrogradely labeled cells in LP), with the exception of LM/PM, which had 8.5% overlap (Figure 3.3). In addition, we completed a complementary pilot experiment employing a novel combination of a virus with efficient retrograde transport of Cre recombinase (HiRet-Cre; Hirano et al., 2013) into PM and AAV1-FLEX-GFP into LP, which also illustrated remarkable specificity in the axonal projections from LP to cortex, projecting only to PM (Figure 3.4).

Discussion

As clearly demonstrated here, the mouse lateral posterior nucleus is topographically organized, with well-segregated zones that communicate specifically with one visual area. As a comprehensive look at the organization of this underappreciated nucleus, this study lays important groundwork for future investigations into LP function, and provides a framework to test theories of thalamocortical circuit organization.

Understanding the anatomy of these loops can lend criticism or credit to various theories about thalamocortical function. A common label for LP/pulvinar is that of a “gate” or “router” for information as it travels through cortex, perhaps for the purposes of synchronization or multisensory processing. With very few LP cells projecting to multiple visual areas (Figure 3.3), this suggests that if LP is a router for information up the visual hierarchy (Olshausen et al., 1993), information must be transferred between cells in LP that project to different regions. Furthermore, the “no strong loops hypothesis” posits that no two brain regions can have reciprocal excitatory, driving connections (Crick and Koch, 1998). It is known that LP receives input from layer 5 of cortex, a putative driving connection (Bourassa and Deschênes, 1995; Kim et al., 2015). According to this hypothesis, cells receiving this driving cortical input should not project back to the same cortical region (presumably to layer 4). Several visual areas, including RL, AL, and AM, receive input from two prominent patches in LP, Po, or VPM. It is possible that these are separate sets of cells that receive driving versus modulatory input, that in return project to different layers, however this needs to be directly tested.

Interestingly, PM is the only area that receives significant input from LPMR (Figure 3.2), and is also the only area we investigated that could be considered a ventral stream visual area based on its physiology (but see Wang et al., 2012). Cells in PM prefer high spatial frequency, low temporal frequency, are tuned for low speeds, and exhibit relatively low direction selectivity (Andermann et al., 2011; Marshel et al., 2011; Roth et al., 2012). V1 neurons that project to PM are tuned similarly (Glickfeld et al., 2013), raising the question of whether LPMR also has functional responses similar to a ventral stream area. In order to further test the idea that LPLR and LPMR are differentially involved in dorsal and ventral streams, we are currently extending these studies to another ventral area, P/POR.

A critical question remains: what are the inputs to these cells? We are actively working to address this question using HiRet-Cre in combination with a G-deleted rabies virus. In the meantime, connecting our observations here to previous studies of the input zones of LP may inform our expectations based on the spatial overlap of inputs and outputs. In cats, LPLR receives input from V1 and does not express acetylcholinesterase, while LPMR receives input from SC and many of the cells there are cholinergic (Abramson and Chalupa, 1988). In rats, the distinction between V1 and SC recipient regions lies along the rostral-caudal axis: rostral LP receives cortical input, whereas caudal LP receives tectal input (Li et al., 2003a). A recent study in mice suggests that LPLR receives input from one class of superior SC cells (Gale and Murphy, 2014a), although there is other evidence that LPMR also receives input from SC (Unpublished data, Allen Brain Institute Connectivity Atlas). Forthcoming experiments will hopefully provide satisfying answers to this question.

Experimental Procedures

Headframe implantation and intrinsic signal optical imaging. All experimental procedures using live animals followed procedures approved by the Salk Institute Animal Care and Use Committee. C57BL/6 mice (1-4 months old) were prepared for imaging by implanting a custom metal headframe as previously described (Garrett et al., 2014; Juavinett and Callaway, 2015). These headframes remained on the mouse for the remainder of the experiment. Before CTB injection, a map of visual cortex was obtained for each mouse using intrinsic signal optical imaging as previously described (Garrett et al., 2014).

Cholera toxin subunit B injection. To trace inputs to visual cortical areas from the thalamus, we used .5% of cholera toxin subunit B (CTB) conjugated to Alexa 488, 555, 594, or 647 (Life Technologies). Mice were anesthetized with 100 mg/kg of ketamine and 10 mg/kg xylazine cocktail via intra-peritoneal injections and mounted in a stereotax (David Kopf Instruments Model 940 series, Tujunga, CA) for surgery and stereotaxic injections. To expose the brain for injection, either a burr hole was drilled or a craniotomy was performed over visual cortex. Injections were done with air pressure using a picospritzer (General Valve Corp, Fairfield, NJ). To prevent backflow, the pipette was left in the brain for 5 minutes before and after injection.

CTB was injected into visual cortical regions based on functional maps overlaid on the blood vessel pattern, using these blood vessels as landmarks. CTB injections into cortex (2-3 per animal) were 20-50 nl for AL, AM and PM, and 40-100 nl for V1, LM and RL, using with 20-40 PSI and a 20-30 μm diameter pipette (Conte et al., 2009). We found these conditions to be optimal in order to restrict CTB to ~300 μm diameter injection sites, a necessary condition for small visual areas. After

recovery, mice were given water with ibuprofen (30 mg/kg) and housed for 4-6 days before tissue harvesting.

Histology. Brains were harvested after transcardial perfusion using phosphate-buffered saline (PBS) followed by 4% paraformaldehyde (PFA). Brains were dissected out from skulls and post-fixed with 2% PFA and 15% sucrose in PBS at 4°C overnight, and then immersed in 30% sucrose in PBS at 4°C before sectioning. Using a freezing microtome, 50 µm coronal brain sections cut and stored in PBS with 0.01% sodium azide at 4°C. Sections were mounted on slides with Polyvinyl alcohol mounting medium containing DABCO and allowed to air-dry.

Image processing. Each section was imaged at 10x using an Olympus BX63 Microscope with parameters adjusted based on the intensity of expression and background fluorescence. The injection sites for each animal were measured to ensure restriction to small cortical visual areas. For LM and RL injections, animals with injection site diameters greater than 500 µm for LM or RL were excluded. For AL, AM, and PM, animals with injection site diameters greater than 300 µm were excluded.

To compute average expression patterns in LP, sections for each visual area were aligned to the Paxinos Mouse Atlas using the Landscape Correspondences macro in Fiji (Schindelin et al., 2012). We determined an appropriate threshold for each section based on the background expression and brightness of label and thresholded by these values to isolate the projection patterns in the thalamus. These images were then smoothed with a Gaussian filter and averaged to compute the mean location of expression in LP for each visual area.

Experiments to determine the number of overlapping cells were imaged at 20x using a Zeiss LSM confocal microscope. For each brain with multiple successful AF-CTB injections, every fourth section was imaged and all cells in LP were manually counted. Percentages reported are the number of cells double-labeled with two different tracers divided by sum of the numbers of cells labeled by each of the same two tracers in LP.

Figures

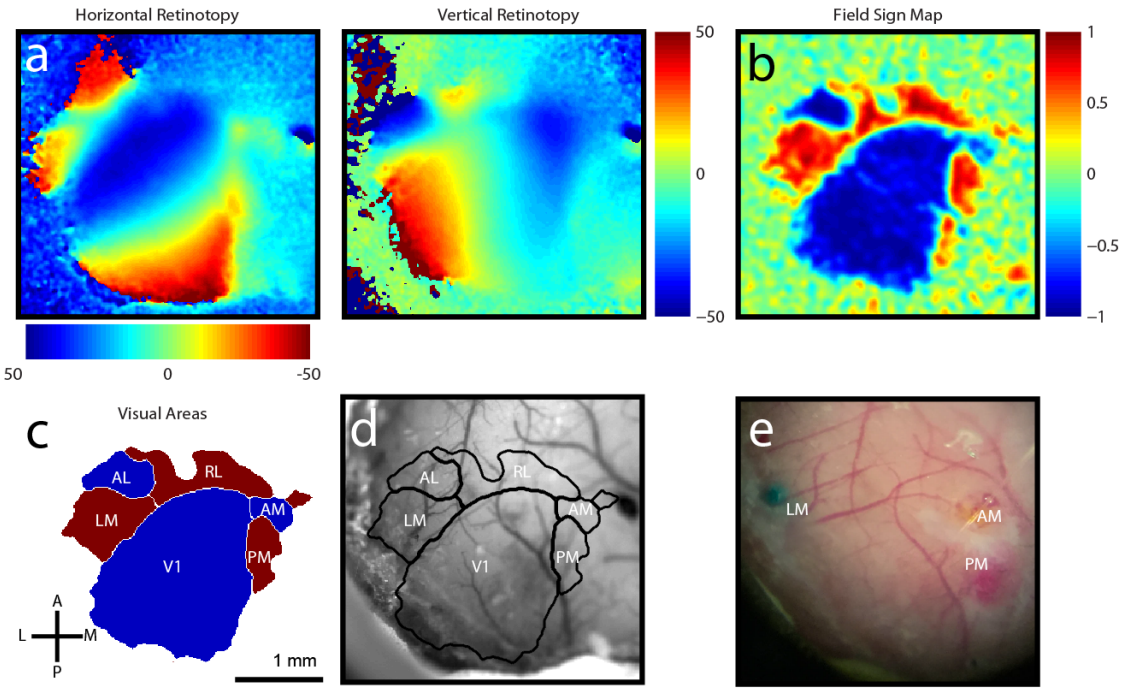

Figure 3.1. Identification of visual areas for AF-CTB injection. a) Example azimuth and altitude retinotopy maps. b) Visual field sign map, computed from the retinotopic maps in (a) as described in Garrett et al., 2014. c) Outline of identified visual areas. Blue areas have a mirror representation of visual space, red areas have a non-mirror representation. d) Visual area borders overlaid on the corresponding blood vessel image acquired with the skull intact. e) Picture of the skull/brain after AF-CTB injection into LM, AM, and PM. Even through the skull, blood vessels and AF-CTB spread are visible.

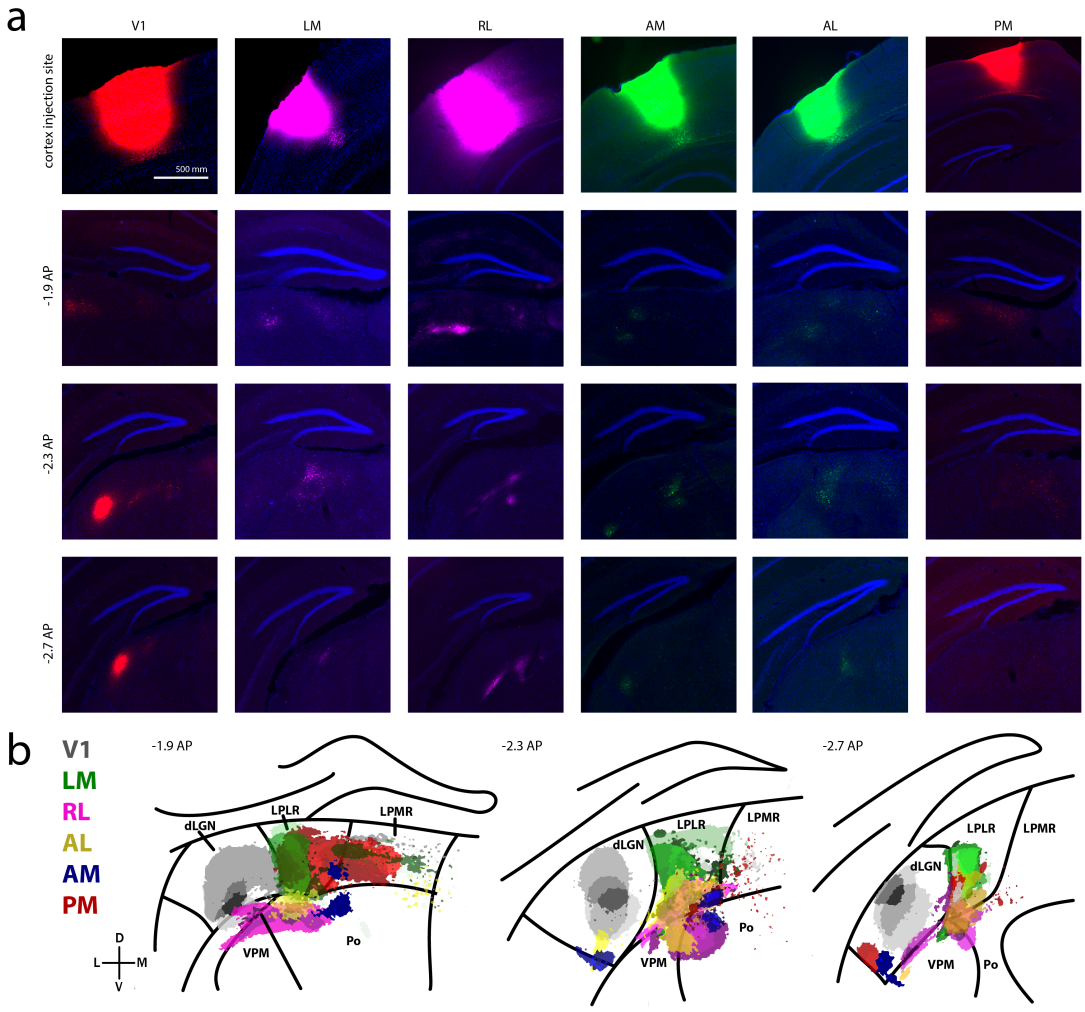

Figure 3.2. Representative injections into six different visual areas and summary diagram. a) Example sections from injections into V1, LM, RL, AM, AL, and PM at three different anterior-posterior locations with either Alexa555-CTB (red), Alexa488-CTB (green), or Alexa647-CTB (pink). Top row shows cortex injection site, imaged with the same parameters as the thalamus. b) Average expression patterns for each visual area, determined by aligning all sections to atlas, thresholding each image, and averaging across injections in the same visual area.

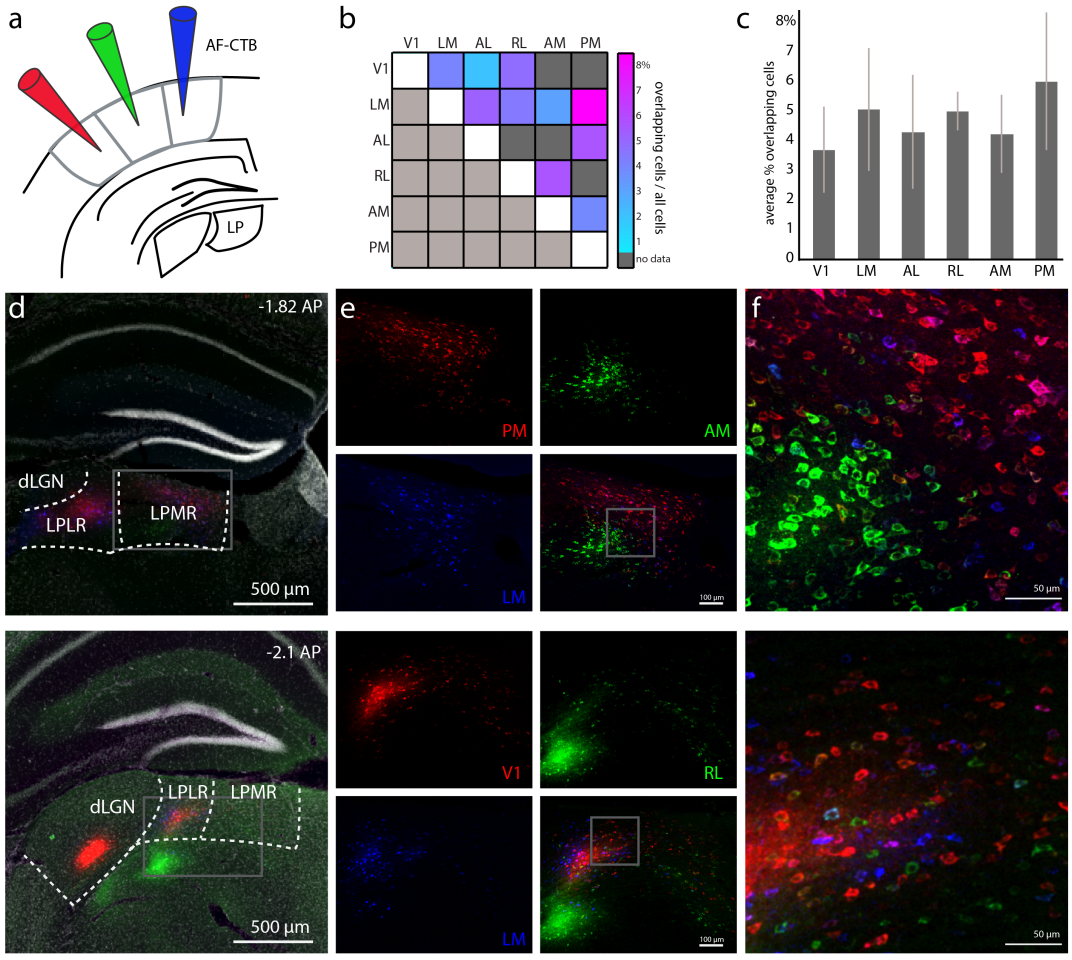

Figure 3.3. Confocal imaging of experiments with multiple tracers to determine percentage of cells projecting to multiple visual areas. a) Demonstration of experiment, where three different AF-CTBs are injected into different visual areas. b) Quantification of overlap between visual areas. Percentages shown are # overlapping cells / total # cells in LP. c) Average percent overlap for each visual area with all other visual areas. Error bars are SEM. d-f) Two sample experiments, demonstrating very little overlap of projection regions in LP, even for spatially overlapping expression patterns. d) Low resolution image to demonstrate location of expression. e) High resolution confocal images of LP for three different injections in cortical regions in the same mouse. f) Inset from (e) to demonstrate overlap.

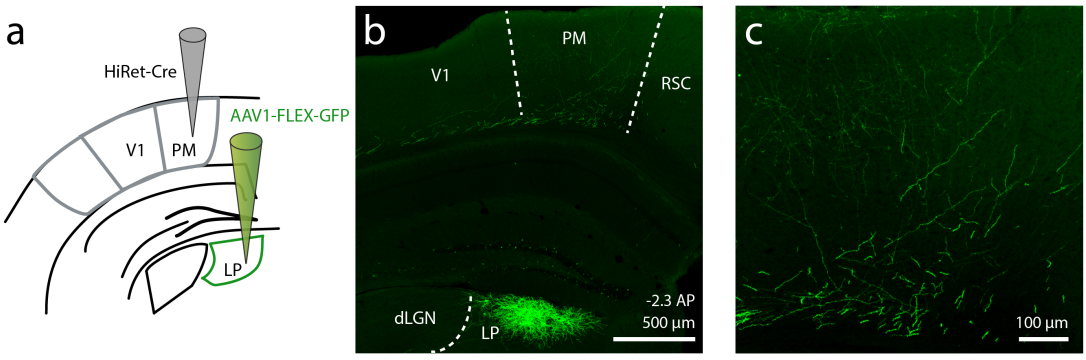

Figure 3.4. Complementary experiment demonstrating specificity of axonal projections from LP. a) Experiment overview, in which a retrograde virus, HiRet-Cre, was injected into PM, effectively expressing Cre recombinase in LP projecting cells and allowing for expression of GFP from AAV1-FLEX-GFP. b) Confocal image demonstrating localized expression of GFP in LP and the presence of axons in PM but not surrounding visual areas such as V1. c) High-resolution confocal image of axons in PM, which extended throughout cortical layers.

Acknowledgements

I would like to thank Euiseok Kim for advice on viruses and the experimental protocol, and Hannah Collins for significant support in the histology for this project. This work was supported by the NIH grants EY022577, EY019005, and MH063912 and the Gatsby Charitable Foundation (E.M.C.). A.L.J. is supported by the National Science Foundation and Martinet Foundation. E.M.K. is supported by the Howard Hughes Medical Institute Gilliam Fellowship and the University of California, San Diego Medical Scientist Training Program T32 GM007198-40.

References

Abramson, B.P., Chalupa, L.M., 1988. Multiple pathways from the superior colliculus to the extrageniculate visual thalamus of the cat. J Comp Neurol 271, 397–418. doi:10.1002/cne.902710308

Allen, A.E., Procyk, C.A., Howarth, M., Walmsley, L., Brown, T.M., 2016. Visual input to the mouse lateral posterior and posterior thalamic nuclei: photoreceptive origins and retinotopic order. J. Physiol. 594, 1911–1929. doi:10.1113/JP271707

Andermann, M.L., Kerlin, A.M., Roumis, D.K., Glickfeld, L.L., Reid, R.C., 2011. Functional Specialization of Mouse Higher Visual Cortical Areas. Neuron 72, 1025–1039.

Bourassa, J., Deschênes, M., 1995. Corticothalamic projections from the primary visual cortex in rats: a single fiber study using biocytin as an anterograde tracer. Neuroscience 66, 253–263. doi:10.1016/0306-4522(95)00009-8

Chalupa, L.M., Coyle, R.S., Lindsley, D.B., 1976. Effect of pulvinar lesions on visual pattern discrimination in monkeys. J. Neurophysiol. 39, 354–369.

Chalupa, L.M., Fish, S.E., 1978. Response characteristics of visual and extravisual neurons in the pulvinar and lateral posterior nuclei of the cat. Exp. Neurol. 61, 96–120.

Conte, W.L., Kamishina, H., Corwin, J. V, Reep, R.L., 2008. Topography in the projections of lateral posterior thalamus with cingulate and medial agranular cortex in relation to circuitry for directed attention and neglect. Brain Res. 1240, 87–95.

Conte, W.L., Kamishina, H., Reep, R.L., 2009. Multiple neuroanatomical tract-tracing using fluorescent Alexa Fluor conjugates of cholera toxin subunit B in rats. Nat. Protoc. 4, 1157–1166.

Crick, F., Koch, C., 1998. Constraints on cortical and thalamic projections: the no-strong-loops hypothesis. Nature 391, 245–250.

Desimone, R., Wessinger, M., Thomas, L., Schneider, W., 1990. Attentional Control of Visual Perception: Cortical and Subcortical Mechanisms. Cold Spring Harb. Symp. Quant. Biol. 55, 963–971.

Gale, S.D., Murphy, G.J., 2014a. Distinct representation and distribution of visual information by specific cell types in mouse superficial superior colliculus. J. Neurosci. 34, 13458–71. doi:10.1523/JNEUROSCI.2768-14.2014

Gale, S.D., Murphy, G.J., 2014b. Distinct representation and distribution of visual information by specific cell types in mouse superficial superior colliculus. J. Neurosci. 34, 13458–13471.

Garrett, M.E., Nauhaus, I., Marshel, J.H., Callaway, E.M., 2014. Topography and areal organization of mouse visual cortex. J. Neurosci. 34, 12587–12600.

Gattass, R., P B Sousa, A., Oswaldo-Cruz, E., 1978. Single unit response types in the pulvinar of the cebus monkey to multisensory stimulation. Brain Res. 158, 75–87.

Gilbert, C.D., Kelly, J.P., 1975. The projections of cells in different layers of the cat's visual cortex. J. Comp. Neurol. 163, 81–105. doi:10.1002/cne.901630106

Glickfeld, L.L., Andermann, M.L., Bonin, V., Reid, R.C., 2013. Cortico-cortical projections in mouse visual cortex are functionally target specific. Nat. Neurosci. 16, 219–226.

Grieve, K.L., Acuña, C., Cudeiro, J., 2000. The primate pulvinar nuclei: vision and action. Trends Neurosci. 23, 35–39.

Hirano, M., Kato, S., Kobayashi, K., Okada, T., Yaginuma, H., Kobayashi, K., 2013. Highly Efficient Retrograde Gene Transfer into Motor Neurons by a Lentiviral Vector Pseudotyped with Fusion Glycoprotein. PLoS One 8, e75896.

Huberman, A.D., Niell, C.M., 2011. What can mice tell us about how vision works? Trends Neurosci. 34, 464–473.

Juavinett, A.L., Callaway, E.M., 2015. Pattern and Component Motion Responses in Mouse Visual Cortical Areas. Curr. Biol. 25, 1759–1764.

Kamishina, H., Conte, W.L., Patel, S.S., Tai, R.J., Corwin, J. V, Reep, R.L., 2009. Cortical connections of the rat lateral posterior thalamic nucleus. Brain Res. 1264, 39–56.

Kamishina, H., Yurcisin, G.H., Corwin, J. V, Reep, R.L., 2008. Striatal projections from the rat lateral posterior thalamic nucleus. Brain Res. 1204, 24–39.

Le Gros Clark, W.E., 1932. THE STRUCTURE AND CONNECTIONS OF THE THALAMUS. Brain 55, 406–470.

Lent, R., 1982. The organization of subcortical projections of the hamster's visual cortex. J. Comp. Neurol. 206, 227–42. doi:10.1002/cne.902060303

Li, J., Bickford, M.E., Guido, W., 2003a. Distinct firing properties of higher order thalamic relay neurons. J. Neurophysiol. 90, 291–9. doi:10.1152/jn.01163.2002

Li, J., Wang, S., Bickford, M.E., 2003b. Comparison of the ultrastructure of cortical and retinal terminals in the rat dorsal lateral geniculate and lateral posterior nuclei. J. Comp. Neurol. 460, 394–409. doi:10.1002/cne.10646

Marshel, J.H., Garrett, M.E., Nauhaus, I., Callaway, E.M., 2011. Functional Specialization of Seven Mouse Visual Cortical Areas. Neuron 72, 1040–1054.

Mason, R., 1978. Functional organization in the cat's pulvinar complex. Exp. Brain Res. 31, 51–66.

Merabet, L., Desautels, A., Minville, K., Casanova, C., 1998. Motion integration in a thalamic visual nucleus. Nature 396, 265–268.

Niell, C.M., 2011. Exploring the Next Frontier of Mouse Vision. Neuron 72, 889–892.

Noseda, R., Kainz, V., Jakubowski, M., Gooley, J.J., Saper, C.B., Digre, K., Burstein, R., 2010. A neural mechanism for exacerbation of headache by light. Nat. Neurosci. 13, 239–245.

Olshausen, B.A., Anderson, C.H., Van Essen, D.C., 1993. A neurobiological model of visual attention and invariant pattern recognition based on dynamic routing of information. J. Neurosci. 13, 4700–4719.

Paxinos, G., Franklin, K.B.J., 2013. The mouse brain in stereotaxic coordinates, Academic Press.

Reep, R.L., Corwin, J. V., 2009. Posterior parietal cortex as part of a neural network for directed attention in rats. Neurobiol. Learn. Mem. 91, 104–113. doi:10.1016/j.nlm.2008.08.010

Roth, M.M., Dahmen, J.C., Muir, D.R., Imhof, F., Martini, F.J., Hofer, S.B., 2015. Thalamic nuclei convey diverse contextual information to layer 1 of visual cortex. Nat. Neurosci. 19, 299–307.

Roth, M.M., Helmchen, F., Kampa, B.M., 2012. Distinct Functional Properties of Primary and Posteromedial Visual Area of Mouse Neocortex. J. Neurosci. 32, 9716–9726.

Schindelin, J., Arganda-Carreras, I., Frise, E., Kaynig, V., Longair, M., Pietzsch, T., Preibisch, S., Rueden, C., Saalfeld, S., Schmid, B., Tinevez, J.-Y., White, D.J., Hartenstein, V., Eliceiri, K., Tomancak, P., Cardona, A., 2012. Fiji: an open-source platform for biological-image analysis. Nat. Methods 9, 676–82. doi:10.1038/nmeth.2019

Sherman, S.M., Guillery, R.W., 1998. On the actions that one nerve cell can have on another: distinguishing “drivers” from “modulators”. Proc. Natl. Acad. Sci. U. S. A. 95, 7121–7126.

Shipp, S., 2003. The functional logic of cortico-pulvinar connections. Philos. Trans. R. Soc. Lond. B. Biol. Sci. 358, 1605–1624.

Sukekawa, K., 1988. Reciprocal connections between medial prefrontal cortex and lateral posterior nucleus in rats. Brain. Behav. Evol. 32, 246–251. doi:10.1159/000116552

Takahashi, T., 1985. The organization of the lateral thalamus of the hooded rat. J. Comp. Neurol. 231, 281–309. doi:10.1002/cne.902310302

Tohmi, M., Meguro, R., Tsukano, H., Hishida, R., Shibuki, K., 2014. The Extrageniculate Visual Pathway Generates Distinct Response Properties in the Higher Visual Areas of Mice. Curr. Biol. 1–11.

Villeneuve, M.Y., Kupers, R., Gjedde, A., Ptito, M., Casanova, C., 2005. Pattern–motion selectivity in the human pulvinar. Neuroimage 28, 474–480.

Wang, Q., Sporns, O., Burkhalter, A., 2012. Network Analysis of Corticocortical Connections Reveals Ventral and Dorsal Processing Streams in Mouse Visual Cortex. J. Neurosci. 32, 4386–4399.